Vilnius University
Faculty of Physics
Institute of Applied Electrodynamics and Telecommunication

Muhammad Umar

INVESTIGATION OF HYBRID SURFACE PLASMON PHONON POLARITONS EXCITED N-GaN GRATINGS AT DIFFERENT CARRIER DENSITIES

Master's Thesis
Electronics and Telecommunications Study Program

Student Muhammad Umar
Academic supervisor Dr. Vytautas Janonis
Director of the Institute Dr. Robertas Grigalaitis

Vilnius 2026

Table of Contents

1. Introduction *2*

Aim of the Study **3**

2. Literature Review *4*

2.1 Polar Semiconductors: Properties and Significance **5**

2.2 Dielectric Function **6**

2.3 Phonons **7**

2.4 Polaritons **8**

2.4.1 Surface polariton dispersion 9

2.4.2 Other Coupling mechanisms 10

2.4.3 Surface Phonon and Surface Phonon–Plasmon Polaritons 13

2.4.4. Numerical Modelling Approaches for Polariton Structures 14

2.4.5 Hybrid SPPhP damping, linewidth, and quality factor 15

2.4.6 Controlling features by changing fill factor 16

2.5 Applications of Surface Phonon–Polaritons in Infrared Spectroscopy **17**

3. Research Methodology *19*

3.1 Materials and Investigated Samples **19**

3.2 Fabrication and Morphological Characterization **19**

3.3 Experimental Method **21**

3.4 Numerical Method: Rigorous Coupled-Wave Analysis (RCWA) **24**

3.5 Data Processing and Comparison Strategy **25**

4. Results and Discussion *26*

5. Conclusion *43*

6. References *44*

1. Introduction

The wide range of applications in thermal imaging, spectroscopy, chemical sensing, selective emitters, radiative cooling, energy-related photonic devices make infrared photonics an important research area of interest[1]. For such applications, the capability to control electromagnetic radiation at subwavelength scale is especially useful, allowing the optical field to be finely tuned in terms of its spectral location, bandwidth, directionality and confinement[1], [2]. One of the best ways to do this control is by the polaritons excitation at material interfaces by employing surface-bound electromagnetic excitations. These surface polaritons are important relevant because they are made up of coupling of electromagnetic waves with collective oscillations inside the material[2].

Free carriers introduced through doping contribute to the plasmonic part of the dielectric response in GaN[3]. Because of this, the optical phonon modes of the polar lattice can couple with free-carrier plasmon oscillations[3], [4]. When this coupling occurs at a patterned surface, it gives rise to hybrid surface plasmon–phonon polaritons (SPPhPs), in which the electromagnetic field is linked with both lattice vibrations and free-carrier motion[3], [5]. These hybrid modes are important in this work because their spectral position, linewidth, damping, and coupling strength can be influenced by changing the doping level and the surface geometry[3], [5].

It is difficult to directly observe these surface-bound hybrid SPPhPs since they do not couple efficiently to the far field without momentum matching[3]. Therefore, there are periodic surface structures, like gratings or surface lattices, necessary[5], [6]. The structures provide in-plane momentum to scatter the bound modes into detectable radiation. The resonating response, however, is extremely sensitive to the structural parameters like period, filling factor, the height of the grooves and the geometry of the grating (linear or circular)[7]. The spectra are also strongly angle dependent and hence both the experimental geometry under which the spectrum was collected and the way the angle is treated in the calculation are important for a meaningful comparison between measurement and calculation[3], [7].

One of the recurring difficulties is that the results of theory and experiment do not always agree[3]. Most numerical methods, like Rigorous Coupled-Wave Analysis (RCWA), assume idealized conditions, ideal periodicity, ideal dielectric functions and defined optical parameters, but real fabricated samples have imperfections such as irregularities in the grooves, sidewall inclination, surface roughness, contamination, etc can broaden or shift the spectral features. Furthermore, FTIR spectrometers are able to record radiation within a limited angular aperture, rather than at a specific angle. This means that although the overall spectral features are matched, fine detail, including the position, width and height of peaks may not always be well matched[3]. The present work aims at this understanding and analysis of the discrepancies.

This thesis focuses on the experimental study of the thermal-emission spectroscopy of hybrid surface plasmon–phonon polaritons in differently doped GaN surface gratings and the theoretical modelling of them using RCWA. To understand the effect of the doping level, two different n-type GaN samples (Sample 1 and Sample 2) are studied with linear and circular surface gratings.

Aim of the Study

This study aims at investigating the behavior of the hybrid surface plasmon–phonon polaritons which are excited in differently doped GaN surface gratings and to evaluate the effect of the doping level, the filling factor, the grating geometry, and the angular field of view on their spectral behavior, both experimentally and theoretically.

To achieve this aim, the following specific tasks are addressed:

- To investigate the angular dependence of the resonant features in the experimentally relevant small-angle range.
- To calculate theoretical spectra and contour maps for the investigated grating geometries.
- To compare experimental and theoretical results for Sample 1 and Sample 2.
- To evaluate the influence of doping level, filling factor, and grating geometry on the excitation of hybrid SPPhP modes.
- To evaluate the causes of theory–experiment mismatch, including finite angular collection, fabrication imperfections, and uncertainty in model parameters.

The importance of this work is that it is a direct comparison of two different doping levels, it considers both linear and circular grating geometries, and it systematically investigates the filling factor. The small-angle spectra and contour maps highlight the local angular behaviour of the resonances particularly. Furthermore, there are no discrepancies between theory and experiment, but rather it is a primary element of the physical interpretation. The thesis adds to the fundamental knowledge of hybrid SPPhP modes in GaN and to the methodological best practices in comparing modelling and measurement in hybrid SPPhP.

2. Literature Review

Infrared photonics is an important part for many applications like, spectroscopy, thermal imaging, chemical sensing, selective thermal emitters, and energy-related photonic devices. In this domain, polar semiconductors such as GaN are particularly relevant because their infrared phonon resonances can support surface polaritonic modes. In doped GaN, the presence of free carriers adds a plasmonic contribution to the material response. This makes it possible to form hybrid surface plasmon–phonon polaritons at patterned surfaces, which is the focus of this work.

Hybrid surface plasmon–phonon polariton emission from n-type GaN surface gratings has already been investigated by Janonis and co-workers. In their 2020 study, polarized reflection and emission spectroscopy were combined with numerical modelling to study n-type GaN gratings for coherent thermal-source applications[6]. Their work showed that patterned n-GaN can support thermally excited hybrid SPPhP modes and that the grating geometry plays an important role in coupling these modes to the far field. Later, Janonis et al. investigated the spatial coherence of hybrid SPPhPs in shallow n-GaN surface-relief gratings and found that the grating period strongly affects the coherence properties. In particular, the 22 μm period grating showed the highest coherence, with experimental and theoretical coherence lengths of about 1.6 mm and 2.3 mm, respectively[5]. More recently, directive and coherent thermal emission from hybrid SPPhPs was studied in n-GaN gratings with linear and radial geometries, showing that grating geometry can strongly influence the directionality and visibility of the emitted radiation [7].

However, some details of the measured emission spectra are still difficult to explain completely. The experimental spectra are influenced by the finite angular collection range of the FTIR setup, while numerical models such as RCWA usually assume idealized grating profiles, periodicity, and optical material parameters. Because of this, the general resonance positions may agree, but the exact peak position, linewidth, intensity, and shape can differ between experiment and calculation. This creates a need for a more careful comparison of measured and simulated spectra, especially close to normal emission where small angular effects may still influence the observed spectral features.

This thesis continues from the previous work by studying more detailed thermal-emission profiles of differently doped n-GaN surface gratings under near-normal collection conditions. The aim is not only to observe SPPhP-related resonances, but also to explain the nature of the observed features by analysing the effects of doping level, filling factor, grating geometry, and angular treatment in RCWA calculations. In this way, the work moves from demonstrating coherent polariton emission toward understanding why specific spectral peaks appear, shift, broaden, or differ between experiment and theory.

2.1 Polar Semiconductors: Properties and Significance

Polar semiconductors are the constituent atoms have a noticeable electronegativity difference, leading to partially ionic bonding. This polarity gives the crystal lattice a dipole-like character and strongly influences its optical and electrical behaviour[8], [9]. In the present work, GaN gives a clear example of polar semiconductors, on which different works have been based for optoelectronic and high-power electronic applications[10],[11].

This is the splitting between the longitudinal optical (LO) and transverse optical (TO) phonon modes, commonly referred to as LO-TO splitting. This splitting occurs because of long-range Coulomb interactions in the polar grating and can be observed using infrared spectroscopy[8], [9]. The interaction between lattice vibrations and electromagnetic waves in these materials also produces the Reststrahlen band, which is the high-reflectivity spectral region between the TO and LO phonon frequencies. In this region, phonon-polariton modes can be supported [9], [10]. GaN relevant to this study because their phonon resonances lie in the infrared range, where they can be investigated using FTIR spectroscopy[9], [11]. In doped GaN, changing the carrier concentration can further modify the dielectric response and allows the plasmon–phonon interaction to be studied under different coupling conditions[3], [4].

Besides their unique optical properties, polar semiconductors have also good electronic properties such as high breakdown electric fields and high saturation electron velocities. These qualities can allow them to be deployed in applications of higher frequency and high power of electronics. Along with those qualities, they also form structures that crystallize and grow along directions noncentrosymmetrically such that it leads in the formation of piezoelectric and pyroelectric properties of those compounds. Such phenomena is widely explored in fields like actuation, sensors and energy harvestings. [8], [9]. In the view of physical properties, they are robust, hard, can survive harsh thermal conditions and the formed surface structures are robust against physical manipulations and damage[7], [8].

In current era’s technological environment, polar semiconductors (GaN) are important part of the modern-day devices. And they are mostly being used in the manufacturing of LEDs, in high electron mobility transistors (HEMTs) and laser diodes. They are the technology of choice for high-power and high-frequency applications like wideband RF amplifiers, power converters, and 5G/6G communication system applications[8], [9].

2.2 Dielectric Function

The dielectric function is the response of a material to an applied electromagnetic field, $\boldsymbol{\varepsilon(\omega)}$. A complex number with a real part that influences dispersion (phase velocity) and an imaginary part that influences absorption (energy dissipation) depending on the frequency. The dielectric function is vital in IR spectroscopy for determining phonon and plasmon resonance frequencies, calculating reflectivity and emissivity, understanding polariton formation in structured materials like surface gratings, etc[12].

There are three basic processes that can occur when a material is exposed to the incident (IR) radiation:

The fraction of light reflected at the surface,

1. **Reflectivity (R): the fraction of light reflected at the surface**
2. **Transmissivity (T): the part of light that passes through the material, and**
3. **Absorption (A): the part of light that is absorbed inside the material.**

In the passive state of no amplification these quantities satisfy the law of the conservation of energy:

$$\boldsymbol{R(\omega) + T(\omega) + A(\omega) = 1} \text{.......................... (1)[12]}$$

where omega(ω) is the frequency which is in inverse centimetre $\boldsymbol{(cm^{-1})}$

The imaginary part of the dielectric function determines the emissivity in polar semiconductor materials. The imaginary part **Im[ε(ω)]** represents optical losses and is related to the refractive index **n** and extinction coefficient **κ** via[12]

$$\boldsymbol{Im[\varepsilon(\omega)] = 2n(\omega)\kappa(\omega)} \text{ .... (2)[12]}$$

The peaks in **Im[ε(ω)]** represent regions of high emissivity due to optical phonon or hybrid phonon–plasmon resonances, which are marked by the characteristic features in the Reststrahlen band [10], [11], [13].

For highly doped n-type GaN, the Reststrahlen band is in the mid-infrared region where the substrate is optically opaque as a result of high absorption and/or the wafer thickness. Therefore, transmittance can be assumed to be zero T≈0 and absorption is approximately equal to

$$\boldsymbol{A(\omega) \approx 1 - R(\omega)} \text{ .... (3)}$$

This features a simple implementation directly from the principle of energy conservation [7], [14].

The law of Kirchhoff's thermal radiation is used to describe the property of a body in thermal equilibrium, where the spectral emissivity at a given frequency equals the absorptivity at that same frequency and temperature:

$$\boldsymbol{\varepsilon(\omega) = A(\omega)} \quad \ldots\ldots\ldots\ldots\ldots\ldots\ldots\ldots\ldots\ldots\ldots\ldots \text{(4)}$$

This relation allows the emissivity of the GaN grating to be obtained directly from the calculated absorption spectrum, and vice versa, under thermal equilibrium conditions[7].

The emissivity **E(ω)** is a measure of the material's ability to emit thermal radiation, which is directly related to the dissipative processes in the material (free carrier excitations and lattice vibrations). If there are no non-linear effects, the absorption is related to the reflectance and transmittance by the following equation:

$$\boldsymbol{E(w) = A(\omega) = 1 - R(\omega) - T(\omega)} \quad \ldots\ldots\ldots\ldots\ldots\ldots \text{(5)[7], [12]}$$

The knowledge of the emissivity of GaN surface gratings is of fundamental importance for thermal emission applications and can be derived from the absorption spectra calculated using RCWA [7].

2.3 Phonons

Phonons, which are the quantum excitations associated with the collective oscillations of atoms in crystal lattices, have significance regarding the mechanical, thermal and optical behaviours of solid materials and how they react to external forces applied to them. In a crystalline material, the atoms oscillate around their equilibrium positions due to thermal motion and this oscillatory motion can be interpreted mathematically as normal modes; therefore, when the normal modes are quantified, they are referred to as phonons.[8].

The mass difference (and charge difference) between the cation and anion sublattices in polar semiconductors GaN and SiC causes strong coupling between optical phonons and electromagnetic waves. This interaction gives rise to several interesting aspects that can be seen in infrared spectra[9], [10]. Due to long-range Coulomb forces between charged ions, optical phonons split into transverse optical (TO) and longitudinal optical (LO) branches[9]:

- **Transverse optical (TO):** atomic displacements are orthogonal to the direction of propagation of the phonon.
- **Longitudinal optical (LO) phonons:** there are atomic displacements parallel to the propagation direction and they interact strongly with the electric field.

The difference in frequency for the LO and TO modes (LO–TO splitting) is directly related to these Coulomb interactions and can be used to monitor the ionic character of the material [9], [10].

Because optical phonons are strongly coupled to the infrared light, there is a spectral region of high reflectivity, referred to as the Reststrahlen band, extending between the TO and LO phonon frequencies[9]. In this band, the real underlying dielectric function is negative which effectively inhibits bulk propagation of electromagnetic waves, allowing only surface phonon polaritons to exist[9], [10]. It is therefore essential to model and understand the infrared spectra of polar materials in the framework of its dielectric function, which contains both TO and LO contributions.[9], [11].

Phonons are not just the cause of the Reststrahlen band but are also involved in the formation of hybrid quasiparticles called phonon-polaritons, which are a combination of optical phonons and electromagnetic waves[2], [10]. The present study of hybrid surface plasmon–phonon polaritons, and especially their surface counterparts in structured GaN gratings essentially focused on these hybrid modes[2].

2.4 Polaritons

Surface plasmon polaritons (SPPs) have been widely investigated in the field of nanophotonics for their ability to localise and guide light below the diffraction limit. This makes them useful for subwavelength optical guiding, transmission, field enhancement and amplification [15]. Although plasmonic effects have been well known for a long time, the current research is still exploring new plasmonic platforms such as metal nanostructures, two-dimensional materials and semiconductor systems with high-mobility electron gases [2], [15].

However, conventional plasmonic materials can exhibit strong damping losses in the terahertz and mid-infrared spectral ranges. A prominent alternative for supporting low-loss, strongly confined infrared modes in the Reststrahlen band are surface phonon polaritons (SPhPs) in polar dielectric and polar semiconductor materials [9], [10]. Hence, SPhPs have been attracting increasing attention in infrared nanophotonics, particularly in polar materials such as SiC and GaN [9], [11].

These surface polaritonic modes are useful in their ability to concentrate electromagnetic fields near the material surface. This feature is important for sensing, integrated photonic circuits, control of thermal emission, and nonlinear optical effects [9], [10]. Nonlinear and active effects associated with SPPs have been investigated for a longer time, however, devices based on SPhPs are still in development especially in the mid-infrared and terahertz ranges [10], [16]. In this context polaritonic platforms provide a compact and tunable route for selective thermal emission, radiative cooling, infrared sensing and future integrated mid-infrared technologies [9], [10].

2.4.1 Surface polariton dispersion

Surface polariton dispersion describes how the frequency of a surface-bound mode change with its in-plane wavevector. In a simple theoretical picture, this can be understood by considering a flat interface between two semi-infinite media. For the present work, the upper medium can be taken as air, while the lower medium is GaN. Since GaN is a polar semiconductor, its dielectric response changes strongly in the infrared region due to optical phonon resonances[9].

Surface polariton modes can exist only when the dielectric conditions at the interface are suitable. In polar semiconductors, this usually occurs inside the Reststrahlen band, where the real part of the dielectric function becomes negative[9], [12]. In this spectral region, electromagnetic waves cannot propagate normally through the bulk material. Instead, they can form modes that remain bound to the surface and travel along the interface, with their electromagnetic field decaying away from the surface. This surface confinement is important for this thesis because the resonances observed in GaN surface structures are linked to these surface-bound optical modes [9].

For a flat interface between two media with dielectric permittivites $\varepsilon_1$and ε_2, the in-plane wavevector of a surface polariton is given by:

$$k_x = k_0\sqrt{\frac{\varepsilon_1\varepsilon_2}{\varepsilon_1+\varepsilon_2}}\text{.................................}(6)$$

Here, $k_x$is the in-plane wavevector of the surface polariton, $k_0$is the free-space wavevector, and $\varepsilon_1$and $\varepsilon_2$are the dielectric permittivities of the two media. In the context of this work, $\varepsilon_1$corresponds to air and $\varepsilon_2$corresponds to the GaN substrate. Because the dielectric function of GaN varies strongly near its infrared phonon resonances, the surface polariton wavevector is also frequency dependent[12], [13].

This relation shows that the surface polariton has a larger in-plane wavevector than freely propagating light at the same frequency. Therefore, a surface polariton is not a normal free-space light wave, but a mode confined to the interface. Its electromagnetic field is strongest close to the surface and decreases exponentially into both surrounding media. This behaviour explains why surface polaritons can provide strong field confinement in the infrared region [12], [13].

In doped GaN, the dispersion is further affected by the presence of free carriers. Along with the optical phonon contribution, these free carriers modify the dielectric response and can shift the spectral position of the supported surface modes[13]. For this reason, comparing differently doped GaN samples is useful for understanding how carrier concentration influences the behaviour of hybrid surface plasmon–phonon polaritons. The discussion of how these surface modes are accessed through patterned structures is kept separate and introduced in the following coupling section.

2.4.2 Other Coupling mechanisms

Surface polaritons are bound to the material interface and usually have a larger in-plane wavevector than freely propagating light at the same frequency. Because of this momentum mismatch, they cannot be efficiently excited or detected from the far field at a perfectly flat surface. Therefore, a coupling mechanism is required to provide the missing in-plane momentum and allow the surface-bound mode to interact with external radiation [9], [19].

The supported polariton modes can be identified by considering both the surface polariton dispersion relation, given in Eq.7, and the momentum-matching condition, given in Eq. 8. The dispersion relation describes the allowed surface-bound modes at the interface, while the momentum-matching condition explains how these modes can be accessed by external radiation. For propagating surface polariton modes, the real part of the substrate dielectric permittivity must be negative and larger in magnitude than that of the surrounding medium. This condition is fulfilled for metals in the plasmonic regime and for polar semiconductors inside the Reststrahlen band [9].

Several coupling mechanisms can provide the additional momentum required for surface polariton excitation. Prism coupling, such as the Otto or Kretschmann configuration, uses total internal reflection to create an evanescent field with a larger in-plane wavevector[19]. Near-field coupling can also excite surface polaritons, because a sharp probe or localized source contains a broad range of spatial momentum components[9], [19]. In addition, surface roughness, defects, edges, and other surface distortions can scatter light and provide extra momentum. Such distortions can act as broadband couplers because they contain many different spatial frequencies, but they usually do not provide precise control over the coupling condition[19].

Fig 1. presents the schematic diagram of the one-dimensional GaN surface-relief grating and the excitation configuration used in this work. The structure consists of a rectangular grating patterned on a GaN substrate with air as the superstrate. The grating is characterized by its period P, grating height $\boldsymbol{H}$, and fill factor $\boldsymbol{FF}$. The period $\boldsymbol{P}$ defines the spatial periodicity of the structure and determines the grating wavevector, which contributes an additional in-plane momentum component. The grating height $\boldsymbol{H}$ represents the modulation depth of the surface profile, while the fill factor $\boldsymbol{FF}$ is defined as the ratio of the ridge width to the grating period and controls the strength of the dielectric modulation within one period[20], [21].

In the Absorption geometry, the incident electromagnetic wave impinges on the grating at an angle φ with respect to the surface normal. The wavevector of the incident light is denoted by $\vec{\boldsymbol{k}}_0$, and its in-plane component is given by $\boldsymbol{k}_0 \mathbf{sin}\,\boldsymbol{\varphi}$, as indicated in the Fig. 1. The incident wave is transverse in nature, meaning that both the electric field vector $\vec{\boldsymbol{E}}$ and the magnetic field vector $\vec{\boldsymbol{H}}$ are perpendicular to the direction of propagation defined by $\vec{\boldsymbol{k}}_0$. For transverse magnetic (TM) polarization, the electric field vector lies in the plane of incidence, while the magnetic field vector is perpendicular to the plane of the drawing and is represented by a filled circle in the schematic [13], [20].

Due to the periodic nature of the grating, an additional in-plane momentum component is introduced by the grating wavevector, where $\boldsymbol{m}$ is the diffraction order. As illustrated in the schematic, the in-plane component of the incident wavevector $\boldsymbol{k}_0 \mathbf{sin}\, \boldsymbol{\varphi}$ and the grating wavevector k_g together define the in-plane wavevector of the surface phonon–plasmon polariton mode, denoted as $\boldsymbol{k}_{\mathbf{SPPhP}}$. The resulting polaritonic mode propagates parallel to the surface, with no out-of-plane component [20].

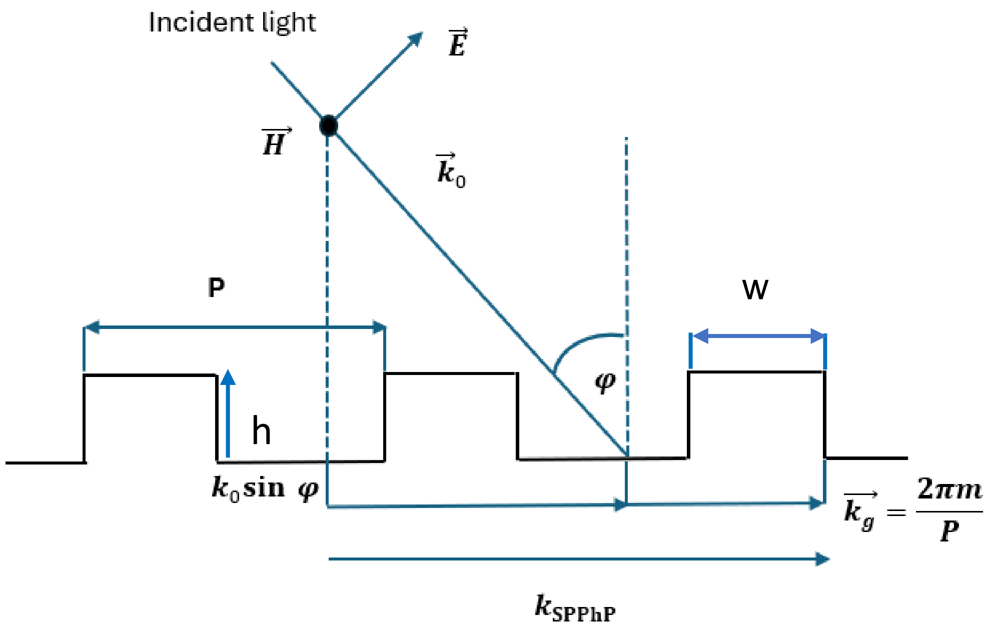

Figure 1:Wavevector representation on surface grating

which represents the momentum condition for the appearance of surface polariton features in grating-based systems [20], [22]. In the RCWA simulations, this geometry is implemented by specifying the grating parameters $\boldsymbol{P}$, $\boldsymbol{H}$, and $\boldsymbol{FF}$, together with the frequency-dependent dielectric function of GaN. The electromagnetic fields and permittivity profile are expanded into a finite number of Fourier harmonics $\boldsymbol{N}$, which determines the numerical accuracy of the solution. Convergence is verified by increasing $\boldsymbol{N}$ until variations in the calculated reflectance and emissivity spectra become negligible. The excitation conditions used in the simulations, including polarization and angle of incidence, correspond to the experimental measurement configuration, enabling direct comparison between numerical and experimental results [22], [23], [24].

In contrast, a periodic grating or surface grating provides a well-defined additional momentum determined by its period. This makes grating coupling more suitable for designing polaritonic structures with controlled resonance positions. For a grating with period P, the grating wavevector is:

$$k_g = \frac{2\pi}{P} \ldots\ldots\ldots\ldots\ldots\ldots\ldots\ldots\ldots\ldots\ldots\ldots \text{(7)}$$

The momentum-matching condition for a grating-coupled surface plasmon–phonon polariton can then be written as:

$$k_{SPPhP} = k_0 \sin\varphi + \frac{2\pi m}{P} \ldots\ldots\ldots\ldots\ldots\ldots\ldots \text{(8)}$$

where k_{SPPhP} is the in-plane wavevector of the surface plasmon–phonon polariton, $k_0 \sin\varphi$ is the in-plane component of the incident or emitted radiation, $m$is the diffraction order, and P is the grating period. This relation shows that the grating period directly controls the additional momentum supplied to the surface mode[19]. At normal incidence, φ=0, so the in-plane momentum of the incident light is zero and the coupling is mainly determined by the grating momentum[19], [20]. In contrast, if the incidence or collection angle does not equal zero, there will be an additional momentum in the in-plane direction due to the presence of the light. The grating-coupled mode can split into two different branches depending on whether the momentum from the light is added/subtracted from the momentum of the grating[20], [25].

And from Fig. 1, fill factor $FF$is defined as the ratio of the ridge width w to the grating period P. It describes the fraction of one grating period occupied by the raised ridge and can be written as[20], [21]:

$$FF = \frac{w}{P} \ldots\ldots\ldots\ldots\ldots\ldots\ldots\ldots\ldots\ldots\ldots\ldots\ldots \text{(9)}$$

The + branch corresponds to the case where the grating momentum and the in-plane light momentum act in the same direction, while the − branch corresponds to the case where they act in opposite directions. As the angle increases, one branch shifts toward higher frequency and the other shifts toward lower frequency. This behaviour appears as angular splitting of the grating-coupled polariton mode[20], [25].

When these branches approach another resonant mode, they may interact instead of simply crossing. This interaction can lead to anticrossing, where the modes repel each other and form two separated hybrid branches. Such splitting and anticrossing behaviour help to identify the coupled nature of the observed SPPhP resonances [20], [25].

This is important for the present work because the GaN surface gratings are designed coupling structures rather than random surface imperfections. While any surface distortion can provide weak broadband coupling, a periodic grating supplies a precise momentum value and allows the polaritonic resonance to be engineered more accurately. Therefore, the periodic GaN gratings used in this thesis make it possible to study how the hybrid SPPhP modes depend on grating period, filling factor, geometry, doping level, and angular collection conditions [5], [6].

2.4.3 Surface Phonon and Surface Phonon–Plasmon Polaritons

To describe the dispersion of surface phonon polaritons given in equation (9) one needs to describe the dielectric function. In the case of phononic excitations it is given by Lorentz type oscillator model as:

$$\epsilon_s = \epsilon_\infty \left(\frac{\omega_{LO}^2 - \omega^2 - i\omega\gamma_{LO}}{\omega_{TO}^2 - \omega^2 - i\omega\gamma_{TO}} \right) \ldots\ldots\ldots\ldots\ldots\ldots\ldots..(10)$$

where ε_∞ is the high frequency dielectric constant of the specific semiconductor, ω_{TO} and ω_{LO} are the TO and LO phonon angular frequencies, and γ is the phonon damping constant [13], [20].

In doped polar semiconductors such as n type gallium nitride (GaN), free charge carriers introduce an additional plasmonic contribution to the dielectric function. This contribution is commonly described by the Drude model and modifies the optical response in the mid infrared region. As a result, the interaction between phonons (undoped material), plasmons (free carriers) and phonons+plasmons (doped semiconductor) leads to hybrid surface phonon plasmon polaritons (SPPhPs), which combine phononic and plasmonic behaviour [20], [21]. A common form of the dielectric function for doped GaN with Lorentz oscillator phononic part and the Drude oscillator model for the plasmonic part is given by:

$$\epsilon_s = \epsilon_\infty \left(\frac{\omega_{LO}^2 - \omega^2 - i\omega\gamma_{LO}}{\omega_{TO}^2 - \omega^2 - i\omega\gamma_{TO}} - \frac{\omega_p^2}{\omega^2 + i\omega\gamma_p} \right) \ldots\ldots\ldots\ldots\ldots\ldots\ldots(11)$$

Where “ ω_p ” is the plasma frequency, and it is important parameter as it directly depends on free carrier’s concentration in doped GaN, which is given by,

$$\omega_p = \sqrt{\frac{Ne^2}{\varepsilon_0 m^*}} \quad (12)$$

N represents the free carrier's concentration, e is the elementary charge, ε_o is the vacuum permittivity and m^* is the electron mass. When the doping level increases the plasmonic part of the dielectric response become stronger and shifted towards higher resonance[25].

The resulting effect of the addition of free carriers changes how much or how little the structure will respond to an optical phonon in addition to how strongly they interact with one another when we mix both types of responses together. The two response types begin to couple and contribute to the overall plasma frequency. If the plasmonic frequency is at or above the LO phonon frequency, they mix in a different way, leading to hybrid responses (i.e. Surface Plasmon-Phonon Polaritons) due to their mutual coupling[6], [25].

SPPhP modes exhibit properties that differ from those of pure SPhPs. Their resonance frequency, linewidth, and field confinement depend not only on the phonon properties but also on the plasmon related parameters such as carrier concentration and damping. Increasing the carrier concentration enhances the plasmonic contribution, which can shift the polariton resonance frequency and modify the damping of the mode. Conversely, reducing or removing free charge carriers leads to behavior closer to that of pure phonon polaritons, with narrower resonances and reduced plasmonic losses [13], [20]. At large doping tunability of the SPPhP modes becomes more pronounced as the region of negative real part of dielectric function in this case spans from TO to LOPC coupled mode, instead of only TO to LO phonon in the case of SPhP[6], [25].

The hybrid nature of SPPhPs provides an additional degree of tunability compared to pure phonon polaritons. By controlling material parameters such as doping concentration, it is possible to tailor the spectral position and coherence properties of the surface polariton modes[6], [20], [25]. This tunability is particularly important for applications involving mid-infrared absorption and thermal emission, where narrowband and controllable spectral features are desired[7], [9], [12] as, with increase of the width of the spectral region of SPPhP formation we increase the operational frequency range of possible SPPhP based device designs[6], [7], [25].

2.4.4. Numerical Modelling Approaches for Polariton Structures

Numerical modeling is essential for the investigation of polaritonic and nanophotonic systems due to a large sensitivity to material dielectric function, geometry, polarization and incidence angle of the probing light. Optical phonons, free carriers, grating coupling and angular dispersion might contribute to measured spectra on infrared transmission for GaN gratings on a substrate. For this reason, numerical methods are useful for connecting the observed spectral features with the physical modes supported by the structure.

Several electromagnetic modelling methods can be used for this type of problem. The finite-difference time-domain method (FDTD) solves Maxwell's equations directly in the time domain by updating the electric and magnetic fields on a spatial grid. It is useful for broadband and transient simulations, but it can become computationally expensive when high spatial resolution or many angle-dependent calculations are required [26]. The finite element method (FEM) is another flexible approach, where the structure is divided into small mesh elements and Maxwell's equations are solved numerically. This method is suitable for complex geometries, although the accuracy and computational cost depend strongly on the mesh quality [27].

The transfer matrix method (TMM) is commonly used for planar multilayer structures, where reflection and transmission through stacked layers are calculated using matrix operations [28]. However, it is less suitable for the present work because GaN gratings have lateral periodicity and diffraction effects, which are not naturally included in a simple planar multilayer model. Other methods, such as the boundary element method (BEM) can be useful for scattering problems and surface-mode calculations, especially when the electromagnetic response is mainly determined by material boundaries [29]. Green's function methods are also useful for studying near-field response, surface-wave propagation, and the local electromagnetic density of states [30]

For periodic grating structures, rigorous coupled-wave analysis (RCWA) is particularly suitable. In RCWA, the periodic dielectric profile and electromagnetic fields are expanded into Fourier harmonics, and Maxwell's equations are solved for different diffraction orders [31] This makes RCWA efficient for calculating diffraction, reflectance, absorption, and emissivity spectra of periodic structures. Since this thesis focuses on periodic GaN surface gratingss, RCWA is selected as the main numerical method for comparing the experimental thermal-emission spectra with theoretical calculations. The detailed RCWA implementation, including grating parameters, dielectric function, polarization, angle selection, and aperture-related angular averaging, is discussed in the Research Methodology chapter.

2.4.5 Hybrid SPPhP damping, linewidth, and quality factor

For hybrid surface plasmon–phonon polaritons (SPPhPs), the total damping is a result of two different loss processes: the intrinsic phonon damping γ_{PH} and the plasmon damping $\boldsymbol{\gamma_{PL}}$**.** Phonon damping γ_{PH} is usually quite small (1-5 cm^{-1}). The phonon damping constant $\gamma_{ph}$is usually relatively small, because optical phonons in polar semiconductors can have comparatively low intrinsic losses. This low damping does not mean that the phonon interaction is weak; rather, it means that the phonon contribution can support sharper and longer-lived resonant features[9], [32]. However, plasmon damping γ_{PL}. is typically larger and significantly sensitive to free-carrier concentration **n**, free-carrier mobility, and impurity, phonon, and interface scattering. The hybrid mode is thus damped with an effective damping rate that depends on the ratio between the phonon frequencies and the plasma frequency **ωp,** which enables the control of the phonon plasmon hybridization degree[6], [25].

In far field measurements (reflectance, absorption or emissivity spectra), the observed linewidth **Δv** (full width half maximum, FWHM) will contain both the intrinsic material losses as described above and the radiative (coupling) losses due to the periodic grating. The grating will allow efficient momentum matching while also allowing for a decay channel back into free-space radiation. A measure of the coherence and sharpness of the resonance, called the quality factor of the resonance[5], [6], is defined as

$$Q = \frac{\nu 0}{\Delta \nu} \quad \text{...(13)}$$

where **v0** is the resonance wavenumber. The narrower resonances, the longer their lifetime, the higher its **Q** value, the better for high resolution sensing and narrow band thermal emission[9], [32].

The narrowest and most coherent SPPhP resonances (**Q>100)** are obtained to optimally exploit the phononic character (which is inherently low loss) and the tunability (induced by plasmonics). When there is no doping, the system returns to pure surface phonon polaritons and can frequently exhibit multiple competing resonances throughout the Reststrahlen band along with reduced spectral purity. If the doping is too high, plasmonic losses take over and broaden the resonance at some point Therefore, studying differently doped GaN surface gratings provides a useful way to investigate how free-carrier concentration controls the damping, linewidth, and quality factor of hybrid SPPhP modes. This is one of the central aims of the present thesis [5], [6], [7].

2.4.6 Controlling features by changing fill factor

One of the important geometric parameters of a surface grating is the fill factor FF. It is defined as the ratio between the ridge width w and the grating period P:

$$FF = \frac{w}{P} \quad \text{...(14)}$$

where $w$is the width of the raised ridge and $P$is the grating period. The fill factor controls how much of each grating period is occupied by GaN and how much is occupied by the surrounding air region.

Therefore, changing FF modifies the effective dielectric contrast of the grating and the spatial overlap between the polaritonic field and the GaN material.

The influence of fill factor on SPPhP resonances is not simply monotonic. A larger fill factor does not always mean a stronger or sharper resonance. Previous studies on n-GaN surface-relief gratings have shown that the resonance frequency, linewidth, and emission amplitude can change in a non-trivial way when the fill factor is varied. For example, in initial surface-relief grating emission studies, the narrowest peaks were observed for $FF25$. When the fill factor was increased to $FF50$, the emission frequency increased and the linewidth also became broader. However, for $FF75$, the feature shifted downward in frequency again, while the emissivity amplitude decreased [6], [7].

This behaviour shows that the fill factor affects several physical processes at the same time. It changes the strength of grating coupling, the effective optical response of the patterned surface, and the radiative damping of the mode. At very low fill factors, the grating perturbation may be too weak to couple efficiently to the surface polariton. At very high fill factors, the structure becomes closer to a nearly continuous GaN surface, so the periodic modulation needed for efficient grating coupling can become less effective. Therefore, an intermediate fill factor can sometimes provide a better compromise between coupling strength, resonance linewidth, and emission amplitude.

In the present thesis, the fill factor is treated as an important design parameter rather than as a simple tuning knob. Together with doping level, grating geometry, and angular collection conditions, it helps determine the spectral position, linewidth, amplitude, and visibility of the hybrid SPPhP resonances. The non-trivial dependence of the resonance features on FF is especially relevant here because this work investigates detailed emission behaviour close to near-normal incidence, where small changes in coupling and angular response can strongly affect the measured spectra [6], [7].

2.5 Applications of Surface Phonon–Polaritons in Infrared Spectroscopy

SPhPs and SPPhPs are significant for infrared spectroscopy since these types of polaritons support microscopic electric fields in the vicinity of the surface. For these polaritons the losses for phononic material like Silicon usually decrease compared to the metallic counterpart (surface plasmon polaritons) in mid-infrared and THz frequency region, and higher Q-factors and narrow resonance linewidths might be beneficial for spectroscopic applications.[9], [12].

In the reflectance, absorption and emissivity spectra, SPPh resonances are sharp, well-defined features that are ideal for extraction of phonon parameters, dielectric response, and free-carrier properties of polar semiconductors[9], [12]. The experimental investigations of infrared absorption spectra of GaN micro and nanostructures have shown intense and sharp infrared absorption peaks corresponding to the propagation and localization of SPPhP modes. The results suggest the surface grating of GaN has great potential for infrared wavelength selective filtering, surface grating based spectral control and high-performance sensing [13].

One important application of these modes is infrared sensing. Since the electromagnetic field of a surface polariton is concentrated near the material surface, the resonance is very sensitive to changes in the local dielectric environment. If an additional material layer, analyte, or contamination is deposited on the grating surface, it can shift the SPhP or SPPhP resonance position. Such resonance shifts can be measured accurately, making surface polariton structures useful for chemical and material sensing applications [9], [12], [13].

Surface polariton structures are also useful for wavelength-selective filtering, narrowband thermal emission, and surface- grating based spectral control. In this context, GaN surface gratings are especially relevant because their resonance position, amplitude, linewidth, and directionality can be influenced by grating geometry, doping level, and angular collection conditions. Therefore, studying SPPhP resonances in structured GaN is important both for understanding hybrid polariton physics and for developing tunable infrared photonic and sensing devices [7], [13].

3. Research Methodology

3.1 Materials and Investigated Samples

The two 500 µm-thick n-type GaN wafers used in the study were chosen to study the effect of the free-carrier concentration on the excitation and optical response of hybrid surface plasmon–phonon polaritons. The two wafers are designated as Sample 1 and Sample 2 where the doping concentration of Sample 1 is approximately **n≈1.55**$\times 10^{19}$**cm**$^{-3}$ and that of sample 2 is approximately **n≈0.42**$\times 10^{19}$**cm**$^{-3}$. These two concentrations were selected with the purpose of sampling a regime where the optical response changes from more phonon dominated to a regime where plasmon–phonon hybridization is significantly enhanced.

Table 1: Sample Parameters

Sample	**Doping concentration (cm^{-3})**	**Crystal orientation**	**Grating type**	**Period (µm)**	**Height (µm)**	**Filling factors investigated**
Sample 1	1.55×10^{19}	c-plane (0001)	Linear and circular	17.5	~1.0	S1CG25FF S1CG50FF S1CG75FF S1LG25FF
Sample 2	0.42×10^{19}	c-plane (0001)	Linear and circular	17.5	~1.0	S2CG25FF S2CG50FF S2CG75FF S2LG25FF

One of the main methodological decisions made in this thesis is the use of two differently doped wafers. This work compares the high-doping and low-doping cases in one material system, both under very similar structural conditions. This enables a direct study of the modification of the position, linewidth and intensity of the hybrid polaritonic modes as a result of the variation in free electron concentration.

On both wafers surface-relief gratings were fabricated as two major geometrical structures: linear gratings and circular/radial gratings. The nominal grating period, the grating height, and the filling factor were 17.5 µm, 1 µm, and 25%, 50%, and 75%, respectively, for all the investigated structures.

3.2 Fabrication and Morphological Characterization

The surface gratings were prepared by conventional UV lithography and chlorine based reactive ion etching (RIE). They were first cleaned and then coated with photoresist and subjected to UV lithography to establish linear and circular grating structures on the surface of the wafers. The pattern was then transferred into the GaN after development using Cl-based RIE to form grooves with a height of ~1 µm.

KH-7700 digital microscope was used to analyze the fabricated structures to confirm the geometry of the grating realized and the possible imperfections visible in the real samples. The images in Fig.2

obtained with the microscope indicated that Sample exhibited distinct surface-relief gratings, which were evident in the form of circles/radials and lines, respectively. The circular structures showed a distinct concentric pattern around the central area, whereas the linear structures displayed regular parallel grooves in the patterned area. Based on these observations, it can be concluded that the desired grating shapes have been successfully fabricated and are appropriate for optical study of hybrid SPPhPs.

The circular gratings have a special area in the center. On Sample 1, centre is a possible local source point for the electromagnetic excitation to couple into a surface polaritonic mode and then propagate radially outward along the concentric grating. While in the linear geometry the polaritonic excitation can propagate mainly along one periodic direction, in the circular geometry it can spread out in many in plane directions following radial symmetry. This is a physically significant point and should be discussed when considering the morphology of the grating.

The Fig, 2. shows representative circular/radial and linear GaN surface gratings fabricated on the highly doped c-plane n-type GaN wafer (Sample 2).The desired periodic geometry is clearly identified and local residues and minor groove irregularities suggest realistic fabrication non-idealises.

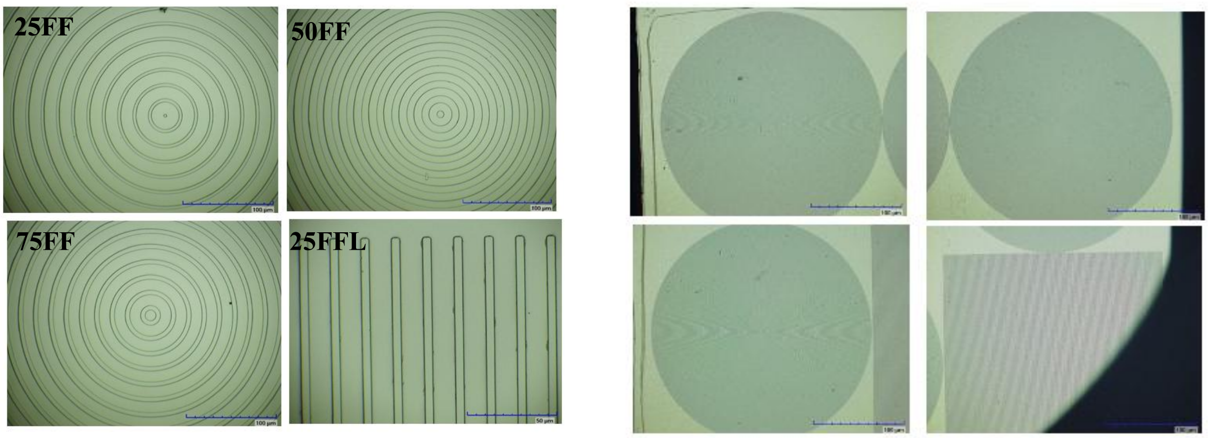

Figure 2:Optical microscope images of the fabricated structures on Sample 2, captured using the KH-7700 digital microscope.

The microscopic images of the linear gratings of the sample 1 and sample 2 shown in Fig. 3. are for the comparison to indicate appearance of slight defects. Since samples with different doping were processed using the same process, but difference in structures was observed, slight calibration of fabrication procedure of low doping samples should be carried out in future fabrication runs.

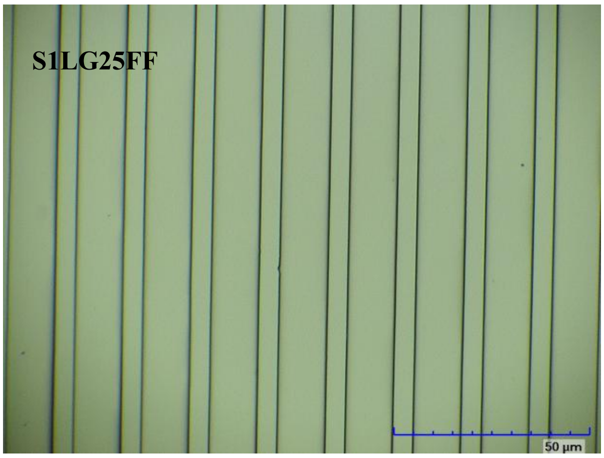

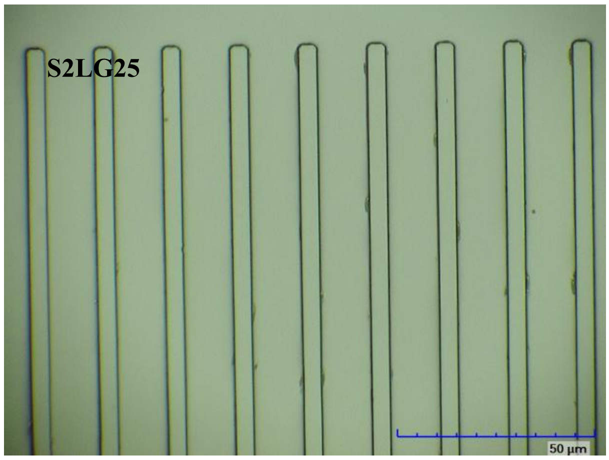

Figure 3: Optical Microscopic image of Linear Gratings For Sample 1 & Sample 2

3.3 Experimental Method

Thermal-emission measurements were carried out using a Bruker Vertex 70 FTIR spectrometer operating in the mid-infrared spectral range.Fig.4. FTIR spectroscopy is commonly used for thermal-emission characterization because it allows broadband infrared spectra to be collected from emitting samples [33]. In this work, the heated GaN grating sample acted as the infrared emitter, and the emitted radiation was collected using an external optical setup before being directed into the spectrometer. Similar FTIR-based thermal-emission approaches have been used to study directional and coherent emission from hybrid SPPhP modes in n-GaN gratings [7].

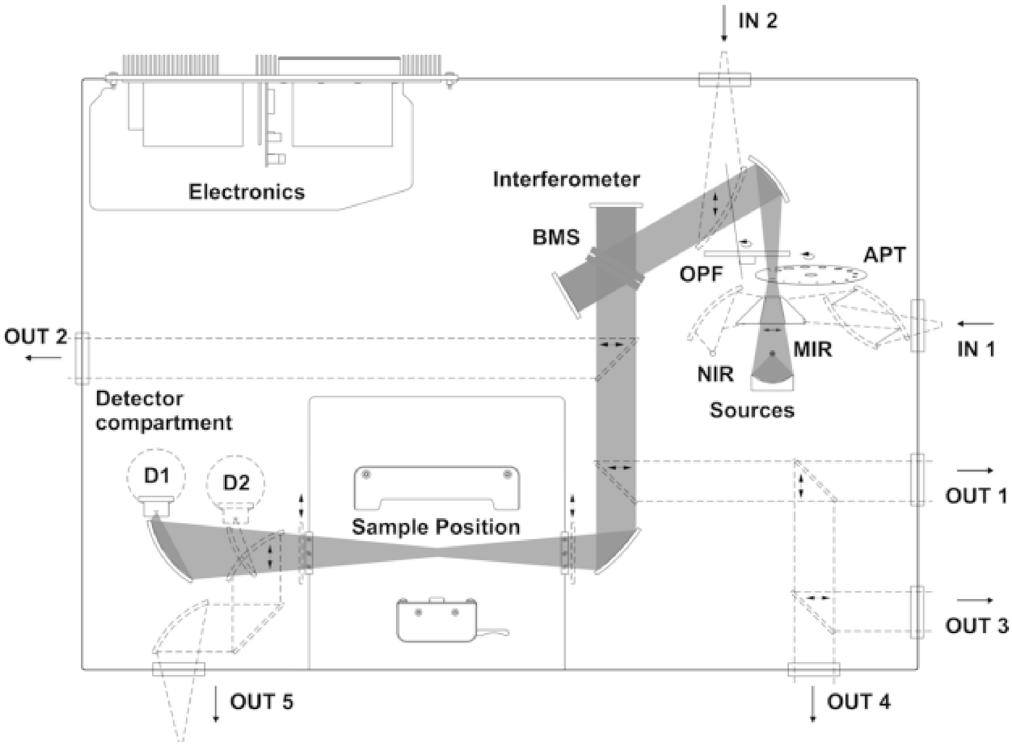

Figure 4: Schematic Diagram of FTIR based Bruker Spectrometer[34]

In the external experimental step-up, shown in Fig. 5, the sample was mounted on a temperature-controlled heater and rotational stage, allowing the emission direction to be controlled during measurement. A parabolic mirror was used to collect the emitted radiation and guide it toward the FTIR input. Since the collected beam was nearly collimated, the finite angular acceptance of the setup was mainly determined by the apertures placed along the optical path. In optical systems, the angular aperture describes the maximum angular range of rays accepted by an optical element or aperture.

A 3 mm aperture was used mainly to suppress parasitic radiation and reduce unwanted background contributions. A 5 mm aperture placed close to the sample limited the active emitting area on the grating surface, while a second 5 mm aperture placed approximately 10 cm away limited the angular aperture of the collected beam. The maximum half-angle can be estimated geometrically as:

$$\theta_{max} = \tan^{-1}\left(\frac{r}{L}\right) \quad (15)$$

here r=2.5mm is the radius of the 5 mm aperture and L=100mm is the distance between the two apertures. This gives:

$$\theta_{max} = \tan^{-1}\left(\frac{2.5}{100}\right) \approx 1.43^\circ \quad (16)$$

Therefore, the approximate full angular aperture is:

$$2\theta_{max} \approx 2.86^\circ$$

cause the effective angular collection is influenced not only by how light is emitted from the source but also by the aperture angle, optical alignment, mirror shape, and optical functions used to collect light, this value should only be viewed as an approximate geometric estimate of angular aperture rather than exact angular aperture. However, this gives the impression that light collected as measured on these spectra corresponded to emission from a small, finite angle (not at a single precisely defined angle)[7].

The samples were typically heated to 500°C, which was sufficient to generate measurable thermal radiation in the spectral region of the GaN Reststrahlen band. In this external-source FTIR configuration, the heated GaN grating acted as the infrared emitter, and the emitted radiation was collected through an open external collection port. FTIR-based thermal-emission measurements have previously been used to study directive and coherent emission from hybrid SPPhP modes in n-GaN gratings [7].

In the present setup, conventional reference-spectrum subtraction and atmospheric suppression by vacuum or purging were not fully applicable because the external source collection path was open. Therefore, atmospheric features such as CO_2 and H_2O had to be considered during interpretation rather than completely removed during measurement. The radiation from the sample was collected as close to a collimated beam as possible, without additional focusing optics directly collecting the sample emission. This is important because the clear observation of the SPPhP-related features under these conditions indicates the strength of the thermal-emission resonances.

The measured spectra were effectively unpolarized because no external polarizer was placed in the FTIR optical path. Therefore, the experimental spectra can contain contributions from both transverse magnetic (TM) and transverse electric (TE) components. This point is important because surface polariton coupling is mainly associated with TM polarization [19]. In TM polarization, the magnetic field is transverse to the plane of incidence and is parallel to the grating lines, while the electric field has a component perpendicular to the grating features, i.e., parallel to the grating vector. This electric-field component is required for efficient coupling to the surface polariton mode [19].

In contrast, in TE polarization, the electric field is transverse to the plane of incidence and parallel to the grating lines. In this case, the electric field does not effectively interact with the periodic modulation along the grating vector, so the structure is seen more like an effective uniform medium. Therefore, TE-polarized radiation is not expected to couple efficiently to the surface polariton resonance. This difference is important because the RCWA calculations in this work mainly describe the TM-polarized response, whereas the experimental spectra contain an unpolarized mixture of resonant TM-like and non-resonant TE-like contributions.

Because SPPhP resonances are angle dependent, the finite angular aperture of the FTIR setup must also be considered when comparing measured spectra with RCWA calculations performed at a single angle. Previous studies on n-GaN gratings have shown that hybrid SPPhP emission is strongly affected by grating geometry and angular collection conditions [5], [7].

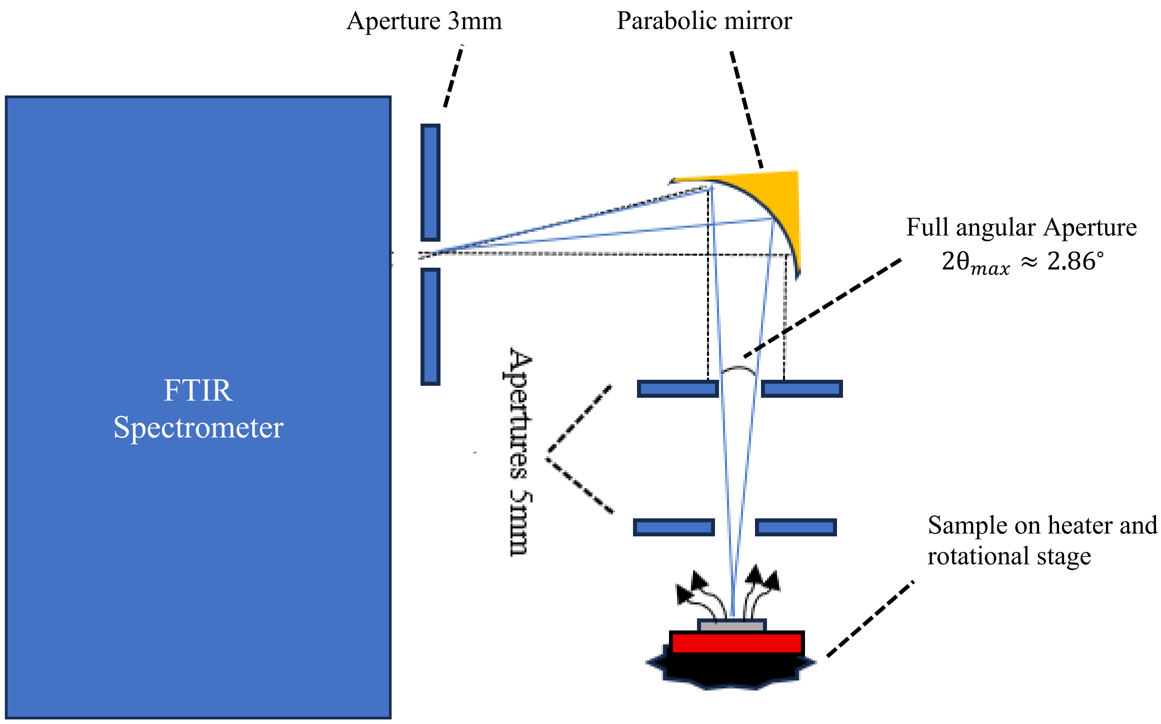

Figure 4: Experimental Setup

3.4 Numerical Method: Rigorous Coupled-Wave Analysis (RCWA)

Rigorous Coupled-Wave Analysis (RCWA) was selected as the main numerical method in this thesis because the investigated samples are periodic GaN surface gratings. RCWA is well suited for modelling diffraction and optical response in periodic grating structures, where the geometry repeats with a defined period. Compared with more general methods such as FDTD or FEM, RCWA is computationally efficient for frequency-domain calculations over many wavelengths, angles, and grating parameters[31].

In RCWA, the periodic dielectric profile of the grating is represented using Fourier harmonics. The electromagnetic fields are also expanded into spatial harmonics, and Maxwell's equations are solved for each diffraction order in the layered structure. From this solution, optical quantities such as reflectance, transmittance, absorption, and emissivity can be calculated as a function of wavelength or wavenumber. This makes RCWA useful for comparing simulated spectra with the experimentally measured thermal-emission spectra[31].

The main input parameters used in the RCWA calculations include the grating period $\boldsymbol{P}$, ridge width $\boldsymbol{w}$, fill factor $\boldsymbol{FF}$, grating height $\boldsymbol{h}$, incidence or collection angle $\boldsymbol{\varphi}$, polarization state, number of diffraction orders, and the complex dielectric function of doped GaN.

The momentum-matching condition was already discussed under literature review by vector representation of grating in Fig, 1. And waveveter equation in (8).

The dielectric function of GaN includes both phonon and free-carrier contributions, allowing the effect of doping level on the hybrid SPPhP response to be included in the model.

The calculations were performed for selected discrete angles in order to study the angular behaviour of the SPPhP resonances. However, the experimental FTIR setup does not collect radiation from one exact angle only. Because of the finite angular aperture of the external optical setup, the measured spectrum represents an angularly averaged response over a small range of angles. Therefore, RCWA spectra calculated at discrete angles were interpreted together with the estimated angular aperture of the experiment. This is important because SPPhP resonances are angle-dependent, and angular averaging can broaden the resonance, shift the apparent peak position, or change the observed intensity[7].

In this thesis, RCWA is therefore used not only to reproduce the main spectral features, but also to understand how the observed SPPhP resonances depend on grating geometry, doping level, polarization, and angular collection conditions.

3.5 Data Processing and Comparison Strategy

Baseline correction and normalization were used to process the experimental spectra, to allow for isolation of the resonant feature and meaningful comparison with the theoretical spectra. The absolute intensities of measured thermal-emission spectra are not directly comparable with the theoretical emissivity scale, so that the comparison was carried out primarily based on the shape of the spectra, position of the resonance, relative intensity and the behavior of the linewidths. This approach is adequate, since the experimental setup contains background contributions, finite angular averaging and the theory is based on an idealized TM-emissivity model.

The final comparison strategy is thus a combination of both experiment and theory in a coherent strategy. The microscope images show the true quality of the fabricated structures, the FTIR measurements give a measured thermal-emission response for Sample 1 and Sample 2, and the RCWA calculations give a theoretical reference response of an idealized structure that helps understand the influence of the elements of the grating's geometry, filling factor, and doping level. The methodology above is an integrated methodology which will be the basis of analysis in the following chapter.

4. Results and Discussion

Sample 1

The first step in analysing Sample 1 was to examine the original thermal-emission spectra measured at different collection angles. Fig, 6, shows the raw emission spectra recorded between 500and 600 cm^{-1}. The spectra show a broad emission background together with a clear spectral feature near the GaN Reststrahlen-band region. A pronounced decrease in emission is observed around the TO-phonon-related region, close to 560 cm^{-1}, followed by a narrow resonance-like feature near 570 cm^{-1}.

In the original spectra, the absolute emission level changes from one angle to another. This variation can come from small changes in collection efficiency, alignment, angular collection, and background contribution. Therefore, direct comparison of the raw spectra is difficult, especially when the goal is to compare the relative strength and position of the SPPhP-related resonance. For this reason, the spectra were later normalized at the TO-level region. This normalization helps to reduce the influence of the broad background and makes the polaritonic feature easier to compare between different angles.

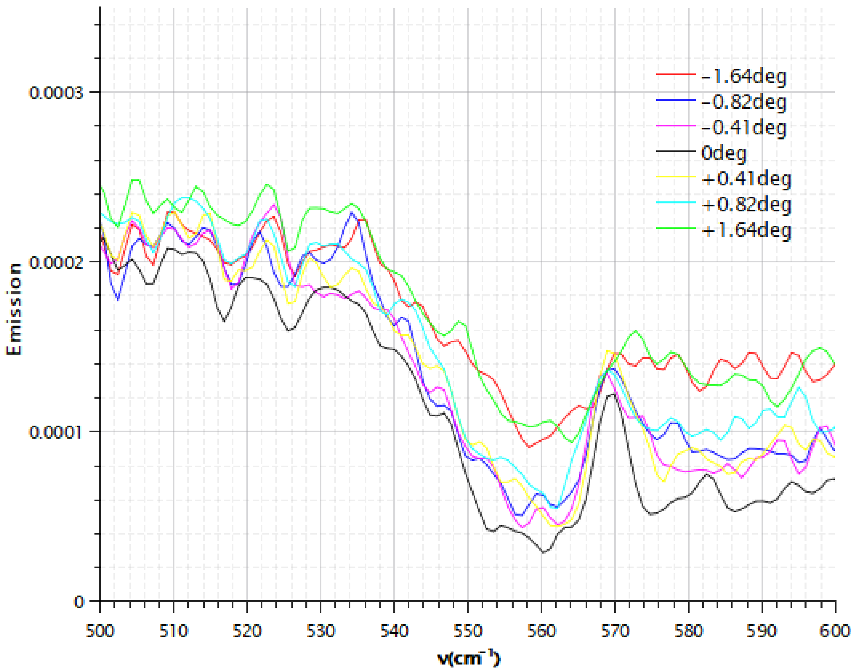

Figure 5:Experimental angular spectra of the 25FF grating of Sample 1

The TO-level region has been used to provide a common reference, which allowed for the normalization of the spectra. Normalized spectra are shown in Fig.7. By referencing spectra to TO, there is a marked improvement in clarity with respect to the general characteristics of the spectra. The broad decrease toward the TO-related region is now better aligned, and the resonance near 570 cm^{-1} becomes more visible for comparison.

This normalization is important because the SPPhP-related peak is relatively narrow and is superimposed on a broader thermal-emission background. By aligning the spectra around the TO-related minimum, the comparison focuses more on the relative resonance behaviour rather than on differences in absolute emission intensity. The normalized spectra show that the peak position remains close to 570 cm^{-1}, while the amplitude and linewidth vary slightly with angle. This indicates that the measured feature is sensitive to angular collection conditions, which is expected for grating-coupled surface polariton modes.

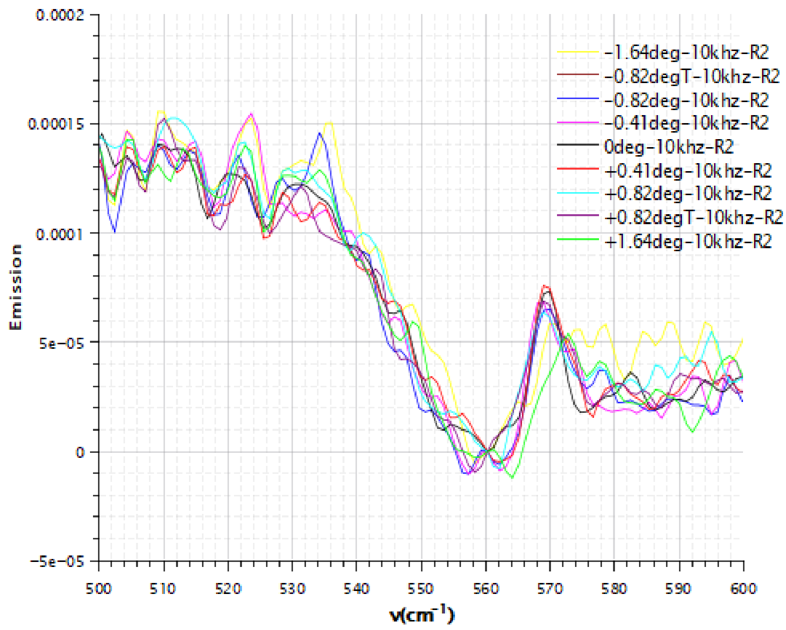

Figure 6:Experimental angular spectra of the 25FF grating of Sample 1, after normalization

For comparison with the experimental spectra, RCWA-based theoretical spectra were calculated using angular averaging. Since the experimental FTIR setup does not collect radiation from one perfectly defined angle, the measured spectrum should not be compared only with a single-angle theoretical curve. Instead, the finite angular aperture of the optical setup must be considered. This is especially important because SPPhP resonances are angle dependent, and even a small angular spread can affect the observed peak position, linewidth, and intensity.

Two theoretical angular averaging ranges were considered: Fig 8, $\pm 0.5°$and approximately Fig 8.1, $\pm 1°$. This Fig 8, $\pm 0.5°$ range was selected to be as appropriate to the conditions of their experiments as possible with the local resonant behavior being investigated in detail under near-normal incidence conditions. Besides single angle/spectra or small angle/spectra, theoretical contour maps were also computed, so as to visualize the local angular dispersion of the hybrid feature. The large-angle maps may be employed for a qualitative illustration or for a comparison of the sort found in literature; the detailed fitting and local comparison used in this thesis are based mainly upon the small-angle interval near normal incidence. This distinction should be explicitly mentioned in the thesis to avoid the reader from getting confused with a wide-angle illustrative map with the main comparison range.

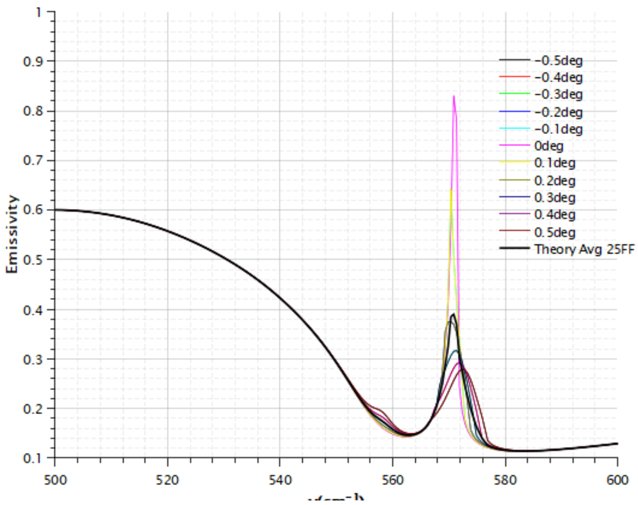

Figure 8: Theoretical RCWA spectra averaged over $\pm \mathbf{0.5°}$.

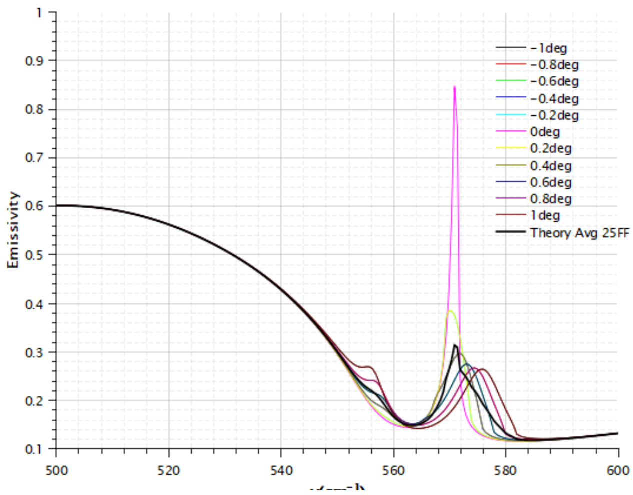

Figure 7.1: Theoretical RCWA spectra averaged over ±1

Fig, 9 compares the experimental spectrum of the 25%fill factor grating with the corresponding theoretical RCWA result. The experimental curve shows a broad decrease toward the TO-related region, followed by a clear resonance close to 570 cm^{-1}. The theoretical curve reproduces the main trend of the spectrum, including the decrease in emission toward the Reststrahlen-band region and the appearance of a narrow resonance.

The agreement between experiment and theory is reasonable in terms of the general spectral shape and the approximate resonance position. However, the experimental curve contains additional fluctuations and a higher background level, especially at higher wavenumbers above the resonance.

These differences are expected because the theoretical model assumes an ideal periodic grating, while the experimental spectrum includes effects from real fabrication imperfections, unpolarized collection, finite angular aperture, and background emission.

For the 25%fill factor case, the resonance appears relatively narrow compared with the broader background. This suggests that the grating provides sufficient momentum coupling while still preserving a relatively sharp polaritonic response. This behaviour is consistent with the idea that lower or intermediate fill factors can support narrow SPPhP features when the coupling strength and radiative loss are balanced.

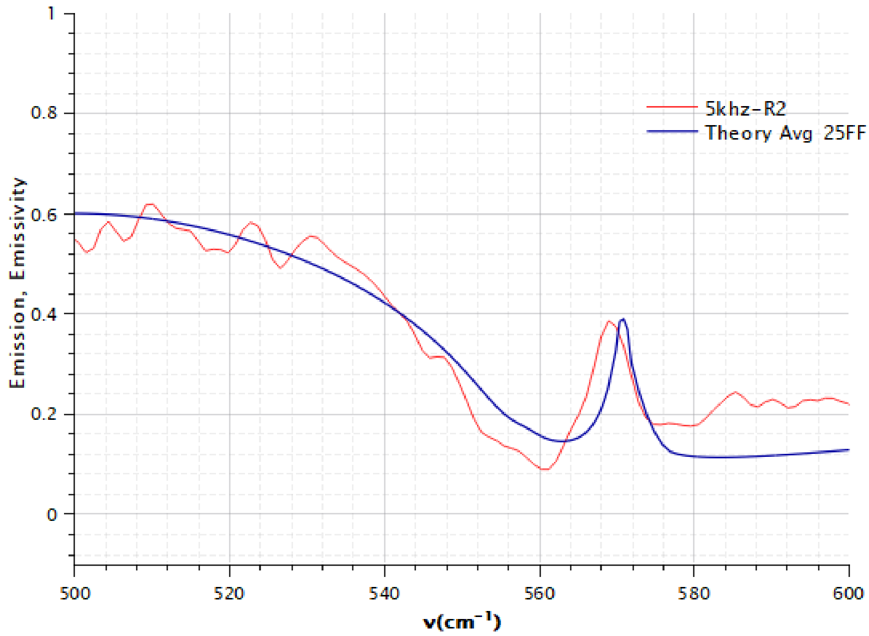

Figure 8:Experimental and theoretical comparison for the 25%fill factor grating of Sample 1

The 25%fill factor linear grating case is shown separately in Fig, 10. In this case, the experimental spectrum shows a stronger broad background and a more pronounced resonance-like feature near $570\ \text{cm}^{-1}$. The theoretical spectrum also predicts a narrow resonance in the same spectral region, but the experimental amplitude and background are higher than the calculated response.

This difference suggests that the measured spectrum is not only determined by the ideal grating-coupled SPPhP mode. Contributions from non-resonant thermal emission, imperfect polarization selectivity, finite angular collection, and slight structural deviations may also influence the measured response. Since the experiment was performed without an external polarizer, the measured signal can include both TM-like resonant contribution and TE-like non-resonant background. This can make the experimental spectrum appear broader or higher than the purely TM-focused theoretical response.

Even with these differences, the presence of a clear resonance close to the theoretically predicted spectral region supports the identification of the observed feature as related to the grating-coupled SPPhP mode.

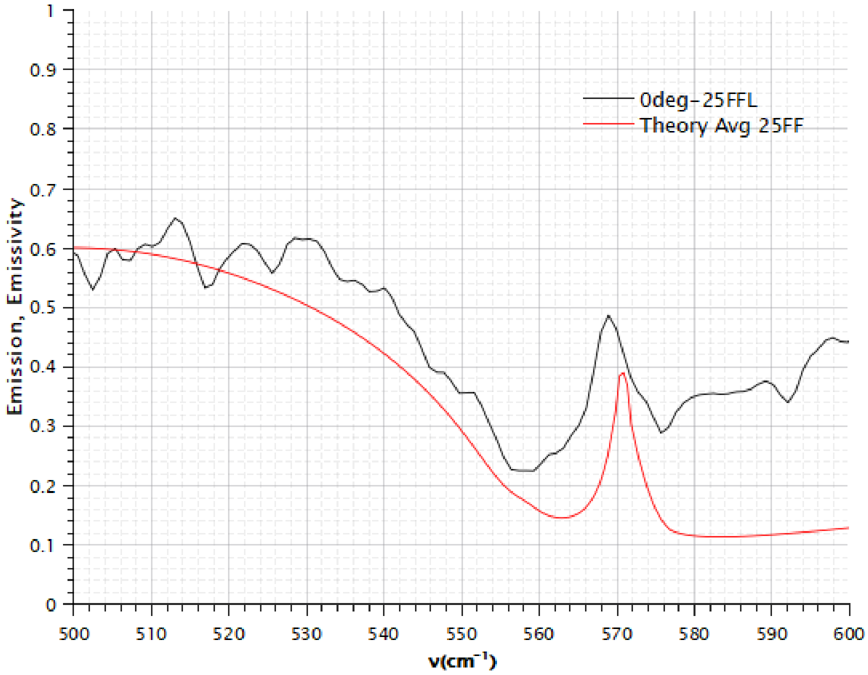

Figure 9:Experimental and theoretical comparison for the 25%fill factor linear grating of Sample 1

Fig. 11. shows the comparison between experiment and theory for the 50%fill factor grating. Compared with the 25%fill factor case, the spectral behaviour becomes more complex. The theoretical spectrum shows a stronger modification of the resonance region, including more pronounced changes around the TO-related minimum and the SPPhP peak. The experimental spectrum also shows a clear change in shape, but the peak position and amplitude do not match the theoretical curve perfectly.

For this fill factor, the grating modulation is stronger because a larger part of each period is occupied by GaN. This changes the effective dielectric contrast and modifies the coupling between the far-field radiation and the surface polariton mode. However, the comparison also shows that increasing the fill factor does not simply increase the resonance strength in a linear way. Instead, the resonance position, linewidth, and background level all change together.

The mismatch between experiment and theory is likely related to the sensitivity of the 50%fill factor structure to fabrication accuracy and angular averaging. Small deviations in ridge width, sidewall shape, or grating height can shift the resonance position. In addition, since the theoretical model is based on an idealized geometry, it may not fully capture the real grating profile. Therefore, the 50%fill factor result shows that fill factor is an important but non-trivial parameter for controlling SPPhP emission.

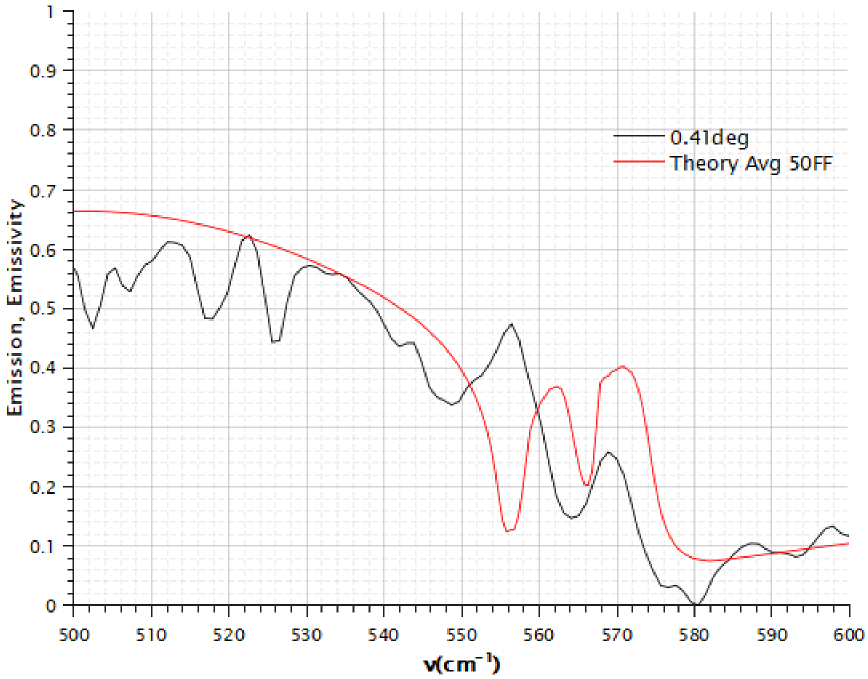

Figure 10:Experimental and theoretical comparison for the 50%fill factor grating of Sample 1

Fig.12. presents the result for the 75%fill factor grating. In this case, the theoretical curve predicts a strong resonance feature at a lower wavenumber region compared with the narrow resonance observed near 570 $cm^{-1}$for the lower fill factor cases. The experimental curve shows a broad emission response and a less sharply defined resonance. The amplitude of the measured feature is also reduced compared with the strong theoretical peak.

This behaviour indicates that the response of the grating does not vary monotonically with fill factor. At high fill factor, the structure becomes closer to a continuous GaN surface, and the periodic modulation becomes less effective in producing a clean and narrow grating-coupled resonance. At the same time, the effective optical response of the grating changes, which can shift the resonance frequency and modify the linewidth.

The 75%fill factor result is important because it shows that a larger fill factor does not necessarily improve the SPPhP resonance. Instead, it can reduce spectral clarity and change the resonance position. This supports the idea that the fill factor must be optimized rather than simply increased. For Sample 1, the comparison suggests that lower or intermediate fill factors give clearer SPPhP-related features than the high fill factor case.

Figure 11:Experimental and theoretical comparison for the 75%fill factor grating of Sample 1

The next phase in the discussion about 25FF is the period comparison. The behavior of the spectrum of the structure with P=17.5µm is more similar with the observation interval (the resonance region) than the case of P=16.5µm. This is physically plausible as it is directly related to the grating period in the momentum-matching requirement for surface-mode excitations. The phase-match condition for free-space radiation and the surface polaritonic mode will change when the period is changed.

This situation is more favorable for 17.5 µm case, which makes the interpretation that this geometry is closer to optimum condition to excite the hybrid mode to be close to the low-damping spectral region. This comparison is especially interesting because it makes it clear that the resonance does not just occur randomly but is strongly modulated by the geometry of the surface- gratings. This is shown in Fig. 13.

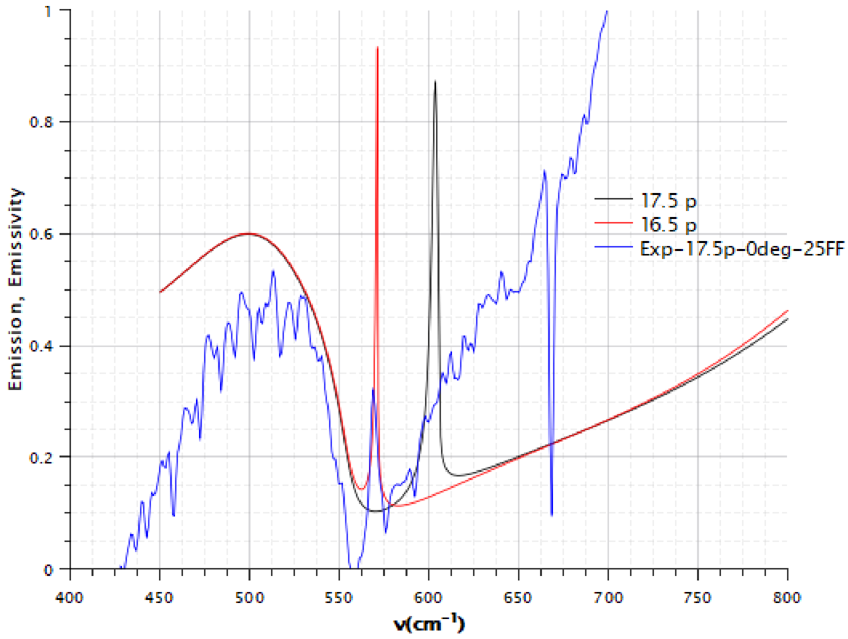

Figure 12:Comparison between the experimental 25FF spectrum at 0° and theoretical calculations obtained for different gratings periods

Sample 2

The original thermal-emission spectra of Sample 2 are shown in Fig. 14 for different collection angles between 0°and 1.64°. The spectra show a broad emission background in the lower-wavenumber region from approximately 500to 540 cm^{-1}, followed by a strong decrease toward the TO-phonon-related region near 558–560 cm^{-1}. A clear resonance-like feature is then observed close to 568–570 cm^{-1}.

The overall shape of the spectra is similar for all measured angles, which indicates that the main spectral response is reproducible. However, the absolute emission level and the strength of the resonance vary slightly with angle. The 0°spectrum shows a somewhat higher background level, while the spectra measured at larger angles show small changes in the minimum near the TO region and in the amplitude of the peak near 570 cm^{-1}. This confirms that the observed feature is sensitive to the angular collection condition, as expected for grating-coupled SPPhP modes.

Because the raw spectra contain different background levels, direct comparison of peak amplitudes is not fully reliable before normalization. Therefore, normalization at the TO-level region is required to compare the polaritonic features more clearly and to reduce the influence of broad thermal-emission background.

After examining the original spectra, the data were normalized using the TO-level region as a reference. This normalization helps align the broad phonon-related minimum and makes the resonance near 570 cm^{-1}easier to compare with the theoretical RCWA spectra. For the theoretical comparison, the 0.41°experimental spectrum was used as the main representative curve because it gives a clear resonance feature while avoiding the slightly higher background level observed at 0°.

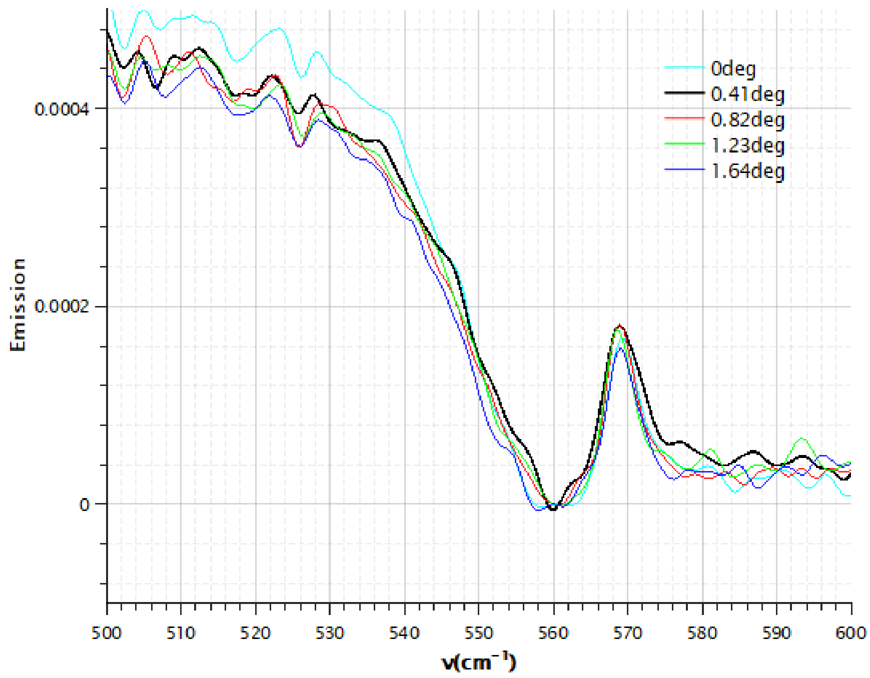

Figure 13: Emission spectra of Sample 2 at 25FF

Fig. 15. shows the comparison between the experimental spectrum and the theoretical RCWA result for the 25%fill factor grating of Sample 2. The experimental spectrum follows the broad theoretical trend quite well from 500to 555 cm^{-1}. Both curves show a gradual decrease in emissivity toward the TO-related minimum, followed by a resonance feature near 570 cm^{-1}.

The agreement is relatively good in the overall spectral shape and in the location of the SPPhP-related resonance. The theoretical resonance is slightly sharper and more pronounced than the experimental one. This difference can be explained by the idealized nature of the RCWA model, where the grating is assumed to be perfectly periodic and the polarization is controlled. In the experiment, the measured spectrum contains both TM-like resonant contribution and non-resonant background, and the finite angular aperture can broaden the peak.

For the 25%fill factor case, the resonance remains relatively narrow and well defined. This suggests that this geometry provides effective grating coupling while keeping the radiative and material losses moderate. Among the Sample 2 results, this case gives one of the clearest agreements between experiment and theory.

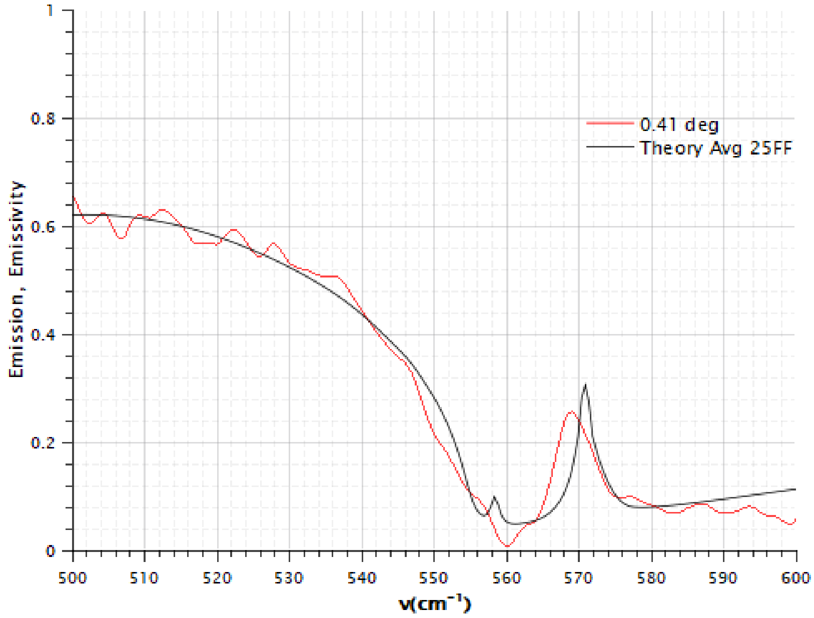

Figure 14:Experimental and theoretical comparison for the 25%fill factor grating of Sample 2

The 25%fill factor linear grating result is shown separately in Fig. 16. The experimental spectrum again shows a broad decrease from the lower-wavenumber region toward the TO-related minimum near 557–560 cm^{-1}. A resonance-like feature is visible close to 570 cm^{-1}, although it is weaker and broader than the theoretical prediction.

The theoretical curve predicts a sharper SPPhP resonance near 570 cm^{-1}. The experimental feature appears at a similar spectral position, but its amplitude is lower. This indicates that the main mode assignment is consistent, but the measured resonance is affected by additional experimental factors. These may include finite angular averaging, slight deviations from the nominal grating profile, surface imperfections, and the absence of polarization selection in the measurement.

This comparison shows that the 25%linear grating supports an SPPhP-related feature, but the resonance is less ideal than the calculated response. The result is still useful because it confirms that the observed peak is not only a background effect; it appears in the same spectral region where the theory predicts a grating-coupled polaritonic mode.

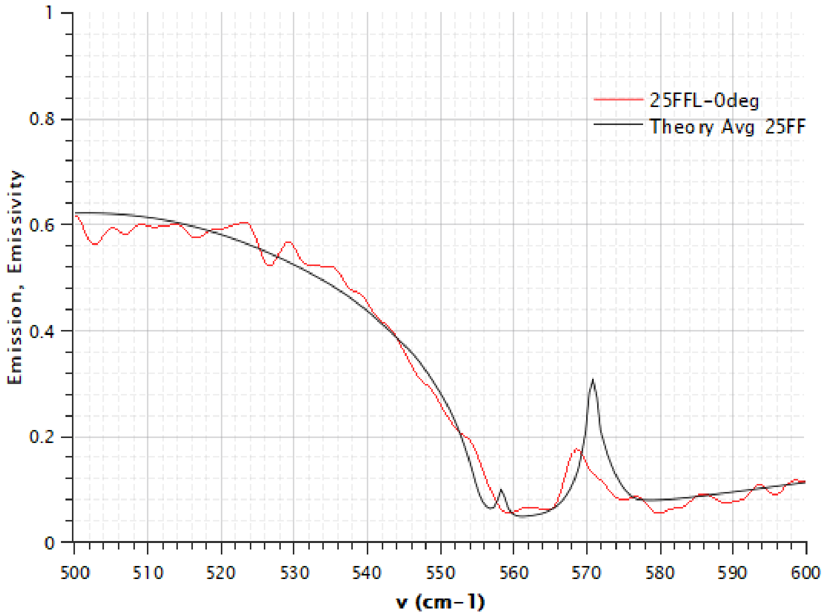

Figure 15: Experimental and theoretical comparison for the 25%fill factor linear grating of Sample 2.

Fig. 17. presents the comparison for the 50%fill factor grating of Sample 2. In this case, the resonance behaviour changes noticeably compared with the 25%fill factor structure. The experimental spectrum shows a stronger feature around 561–563 cm^{-1}, followed by a sharp decrease after the resonance region. The theoretical result predicts two strong spectral features around this region, with a narrow resonance and a second peak at slightly higher wavenumber.

The comparison shows that the 50%fill factor case is more complex than the 25%case. The experimental curve captures the general modification of the spectral shape, but the exact peak positions and amplitudes do not fully match the theoretical response. This suggests that the resonance is highly sensitive to grating geometry and angular treatment. Since 50%fill factor increases the dielectric modulation compared with 25%, it can strengthen the coupling, but it can also increase radiative losses and change the linewidth.

The mismatch between experiment and theory may also come from small fabrication deviations in ridge width, sidewall shape, or grating height. Because the theoretical model uses nominal geometry, even small differences in the actual structure can shift the resonance position. Therefore, the 50%fill factor result shows that fill factor does not control only the peak intensity; it also affects the resonance position, linewidth, and mode structure.

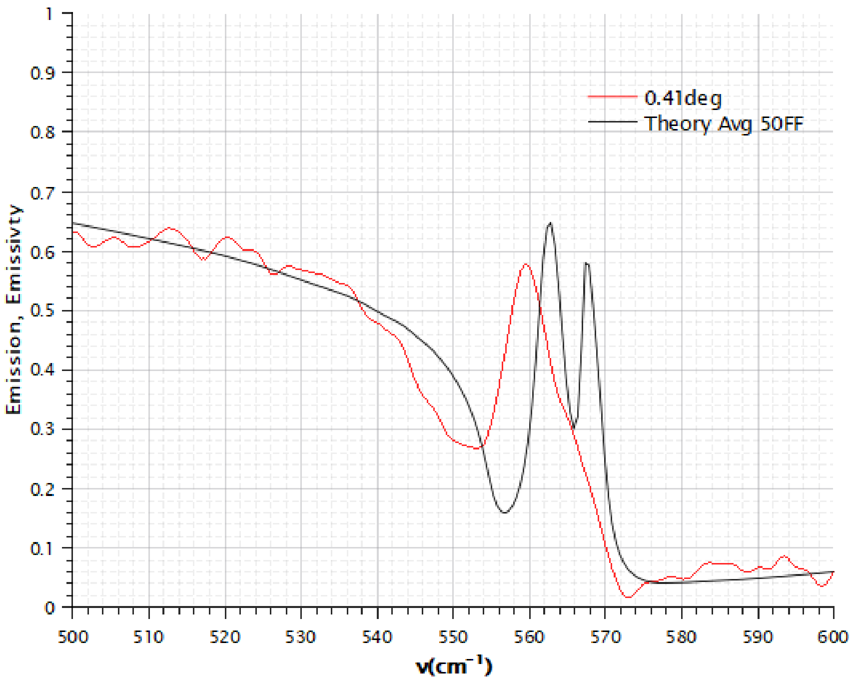

Figure 16: Experimental and theoretical comparison for the 50%fill factor grating of Sample 2.

The 75%fill factor result for Sample 2 is shown in Fig. 18 This case shows the strongest difference between experiment and theory. The theoretical spectrum predicts a very sharp and intense resonance near 560 cm^{-1}, followed by a rapid decrease in emissivity. In contrast, the experimental spectrum shows a broader response with a less sharply defined resonance, and the emission does not follow the same sharp theoretical peak.

This result shows that the high fill factor structure is very sensitive to the exact grating geometry. At 75%fill factor, most of the period is occupied by GaN, so the grating begins to behave more like a nearly continuous surface with a weaker periodic perturbation. At the same time, the remaining groove region becomes narrow, making the optical response very sensitive to fabrication accuracy. Small variations in groove width, sidewall angle, or surface quality can therefore strongly affect the measured spectrum.

The 75%fill factor comparison also supports the idea that the fill factor dependence is non-monotonic. A larger fill factor does not automatically produce a better or cleaner SPPhP resonance. Instead, the resonance can shift, broaden, or lose spectral clarity depending on the balance between grating coupling, radiative loss, and material response.

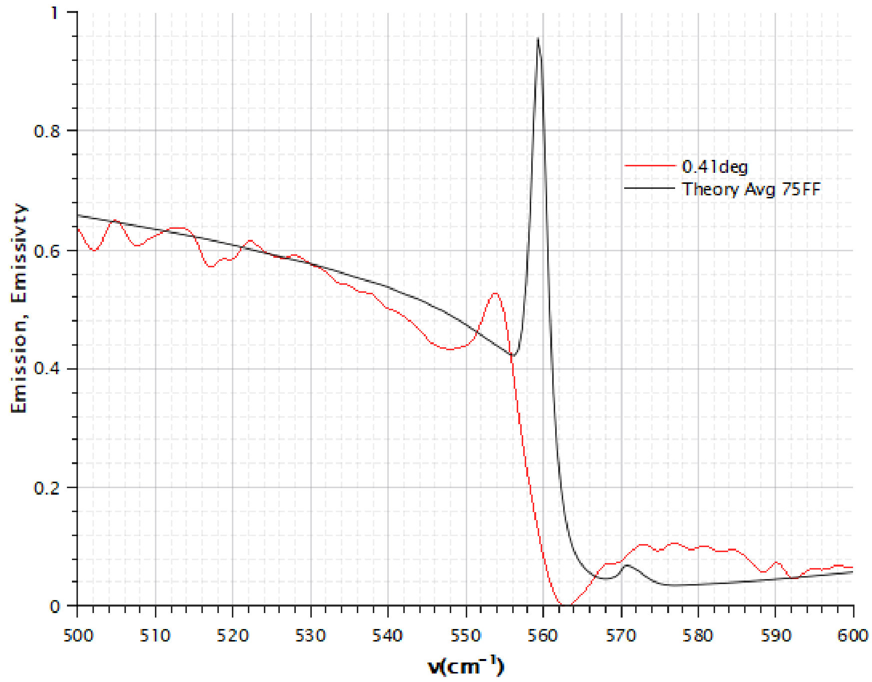

Figure 17: Experimental and theoretical comparison for the 75%fill factor grating of Sample 2

Sample Results Comparison

For the side-by-side comparison of both samples, the fill-factor dependence shows a clear but non-monotonic behaviour. At 25%fill factor, both Sample 1 and Sample 2 show the clearest SPPhP-related resonance close to the GaN Reststrahlen-band region, with reasonable agreement between experiment and RCWA in terms of the general spectral shape and resonance position. Sample 2 follows the theoretical curve slightly better, while Sample 1 shows a higher experimental background and stronger deviation in amplitude. For the 25%linear grating, both samples again show a resonance near the calculated SPPhP region, but the experimental peaks are broader than the theoretical ones, which may be related to unpolarized detection, finite angular aperture, and small fabrication imperfections. At 50%fill factor, the response becomes more complex in both samples: the stronger dielectric modulation changes the coupling condition and modifies the resonance position, linewidth, and amplitude. This shows that increasing the fill factor does not simply increase the resonance strength but also changes the balance between grating coupling and radiative damping. At 75%fill factor, both samples show the largest mismatch between experiment and theory. The theoretical curves predict sharper resonance features, while the measured spectra are broader and less clearly defined. This is likely because a high fill factor makes the structure closer to a continuous GaN surface and makes the narrow groove region more sensitive to fabrication errors, sidewall shape, and surface roughness. Overall, the comparison shows that both samples support hybrid SPPhP-related thermal-emission features, but the best agreement and clearest resonances are generally obtained at lower fill factor, especially around 25%. Therefore, fill factor should be treated as a non-trivial design parameter that affects not only resonance amplitude, but also linewidth, spectral position, radiative loss, and sensitivity to fabrication quality.

Figure 18: Samples Comparison at All Filling Factors

Contour plot Sample 1 theory

For Sample 1, the theoretical TM emissivity contour plots show how the grating-coupled SPPhP modes disperse with angle for different fill factors. In the $FF = 0.25$case, the resonance near $570\ \text{cm}^{-1}$is relatively weak and narrow, with only a slight angular variation around normal incidence. This indicates weaker grating coupling but a more spectrally confined response. For $FF = 0.50$, the contour plot clearly shows two dispersive branches forming the $+$and $-$modes. These branches arise from the momentum-matching condition $k_{\text{SPPhP}} = k_0 \sin\ \varphi + 2\pi m/P$, where one mode corresponds to the addition of light momentum and grating momentum, while the other corresponds to their difference. As the angle increases away from $0°$, one branch shifts to higher wavenumber and the other shifts to lower wavenumber, producing a visible angular splitting and anticrossing-like behaviour near the centre. This indicates stronger coupling and clearer angular dispersion at $FF = 0.50$. In the $FF = 0.75$case, the emissivity feature becomes much stronger and broader around 555–$560\ \text{cm}^{-1}$, but the two branches are less clearly separated. This suggests that the high fill factor increases the overall emissivity and coupling strength but also broadens the resonance and reduces spectral sharpness. Overall, the theoretical contour plots show that the fill factor strongly controls the visibility, linewidth, and angular splitting of the SPPhP modes, with $FF = 0.50$giving the clearest $+$and $-$mode behaviour for Sample 1.

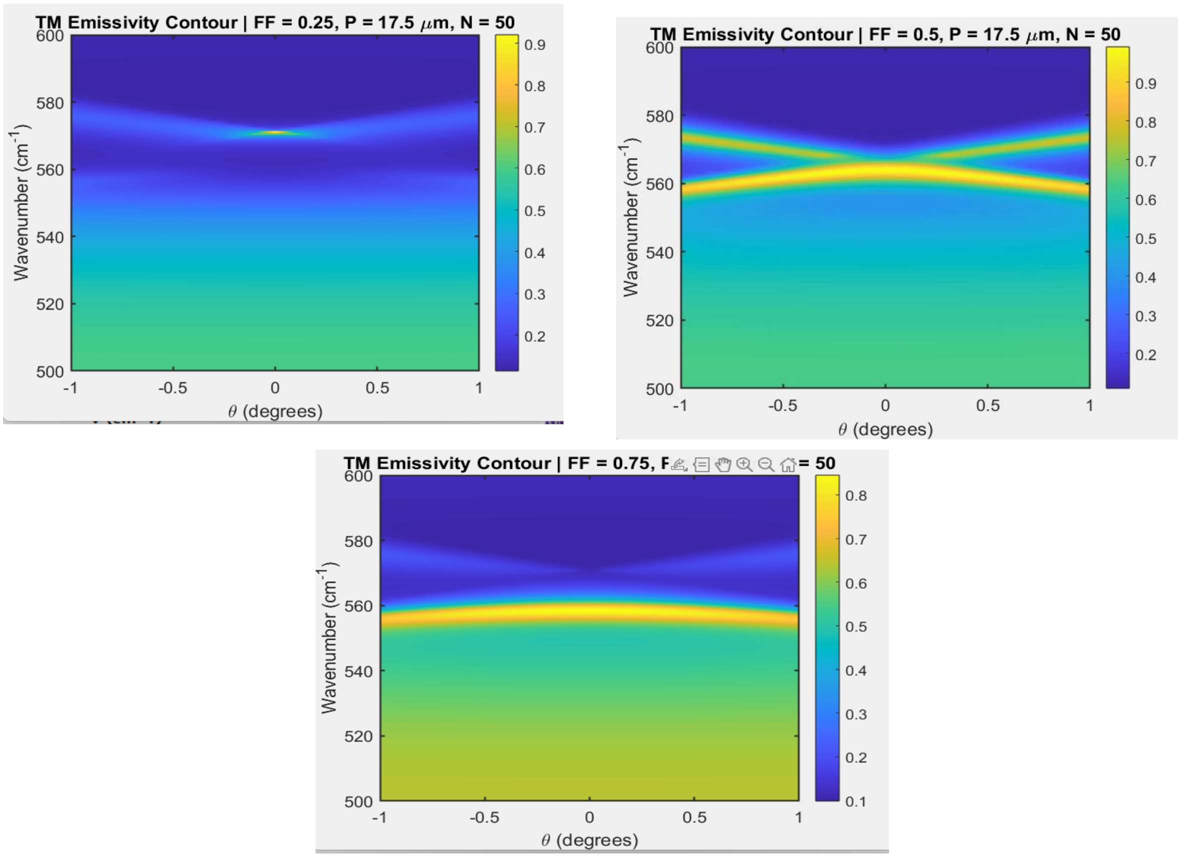

Figure 19: Contour Plots for Sample 1

Contour plot Sample 2 theory

For Sample 2, the theoretical TM emissivity contour plots show that the angular behaviour of the SPPhP modes strongly depends on the fill factor. For $\boldsymbol{FF = 0.25}$, a relatively narrow resonance appears near $\mathbf{570\ cm^{-1}}$, with only weak angular splitting around normal incidence, indicating that the grating coupling is present but not very strong. For $\boldsymbol{FF = 0.50}$, the $+$and $-$branches become much clearer: one branch shifts upward in wavenumber while the other shifts downward as the angle moves away from $\mathbf{0}°$. These branches come from the grating momentum-matching condition, where the in-plane light momentum is either added to or subtracted from the grating momentum. This produces the characteristic angular splitting of the SPPhP mode and shows stronger coupling than in the $\boldsymbol{FF = 0.25}$case. For $\boldsymbol{FF = 0.75}$, the emissivity feature becomes stronger and broader around $\mathbf{555}$–$\mathbf{560\ cm^{-1}}$, but the separate $+$and $-$branches are less clearly resolved. This suggests that the high fill factor increases the overall emissivity and coupling strength but also broadens the mode and reduces spectral sharpness. Overall, the Sample 2 contour plots show that $\boldsymbol{FF = 0.50}$gives the clearest angular splitting of the $+$and $-$SPPhP modes, while $\boldsymbol{FF = 0.25}$gives a weaker but narrower feature and $\boldsymbol{FF = 0.75}$gives a stronger but broader response.

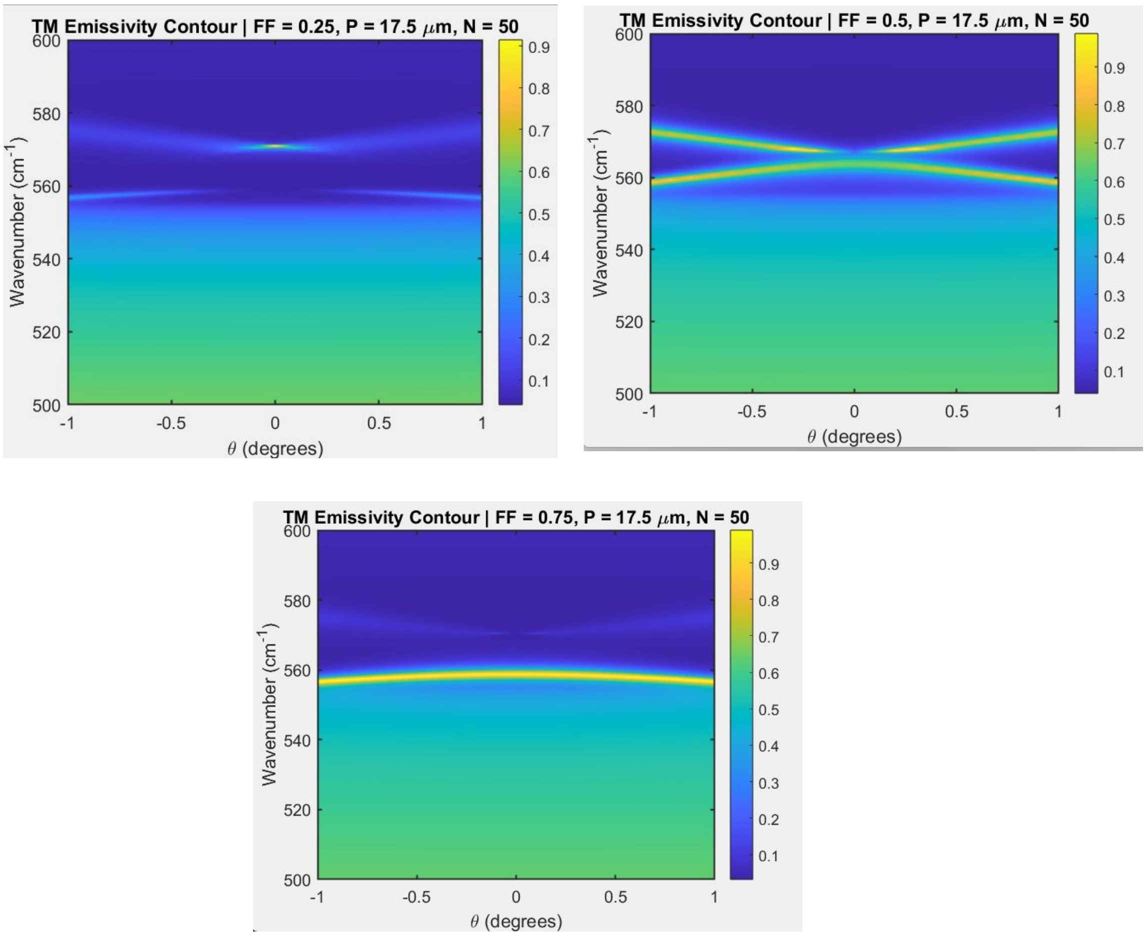

Figure 20: Contour Plots for Sample 2

Table 2. *Summary of theory–experiment comparison*

Case	Theory predicts	Experiment shows	Level of agreement	Main reason for mismatch
Sample 1, 25FF	Narrow resonance near ~570 cm^{-1} with weak local splitting	Clear resonance near same region with broader shape	Qualitative to reasonable	Finite angular collection, normalization, structural imperfections
Sample 1, 50FF	Clearer local branch splitting	Structured resonance with partially merged features	Qualitative	Experimental broadening, unpolarized detection
Sample 1, 75FF	Strong dominant lower branch	Broader dominant resonance	Qualitative	Increased damping and fabrication effects
Sample 2, 25FF	Resonance in correct spectral region	Broader and weaker resonance	Qualitative	Lower doping, weaker hybridization, background effects
Sample 2, 50FF	Two local branches predicted	Broadened structured response	Qualitative	Limited resolution and finite aperture
Sample 2, 75FF	Strong sharp dominant branch	Broader and damped dominant branch	Qualitative	Lower carrier concentration, imperfections, finite-angle averaging

Overall, there are the same general physical conclusions from Sample 2 as with Sample 1, though in a less strongly hybridized regime. The resonant features are found to be angle-dependent, dependence on filling factor, and to generally agree with the contour maps of RCWA, indicating that the lower doped sample still supports hybrid surface plasmon–phonon polaritons. The spectra measured for Sample 2 are, however, generally more broadened, more apparent mismatches exist between theory and experiment and the branch structure is less well resolved in experiment than for Sample 1. This is certainly consistent with the reduced free-carrier concentration of Sample 2 which causes the plasmonic contribution to be smaller and thus decreases the hybridization strength. The best answer to this criticism is that the experimental results, the direct comparisons with the theory and the contour maps all present the same consistent physical picture: Sample 2 still shows hybrid SPPhP behavior, but in a more diffuse, less strong and less well-resolved form than the highly doped sample.

Table 3. *Experimental comparison of resonance behavior for Sample 1 and Sample 2*

Sample	Structure	Filling factor	Approx. resonance position (cm^{-1})	Approx. FWHM (cm^{-1})	Approx. Q-factor
Sample 1	Circular	25%	568	5.79	98
Sample 1	Linear	25%	568	5.11	111
Sample 1	Circular	50%	568	5.47	104
Sample 1	Circular	75%	553	6.67	82
Sample 2	Circular	25%	568	6.5	87
Sample 2	Linear	25%	568	5.12	111
Sample 2	Circular	50%	559	8.7	64
Sample 2	Circular	75%	554	5.39	102

5. Conclusion

- Hybrid SPPhP emission features were observed in both GaN samples in the Reststrahlen-band region, namely between $\mathbf{550}$–$\mathbf{570\ cm^{-1}}$. Sample 1 generally shows stronger and better-resolved features, while Sample 2 shows broader resonances, consistent with its lower free-carrier concentration.
- Fill factor and angular dependence strongly influence the observed resonance behaviour. The results show a non-monotonic dependence on fill factor. The 25FF structures produce the most narrowly defined and high contrast resonance peaks. The 50FF grating emission features exhibit more complex resonance behaviour including double-peak. The 75FF grating emission shifts to even lower frequency on the incoherent radiation edge and exhibits a single peak behavior.
- The filling factor related emission feature trends were explained by the existence of + and – modes in the polariton dispersion, tuning of activity of which was shown to be possible by tuning the filling factor of the grating.
- The RCWA calculations reproduce the main resonance positions, fill-factor trends, and angular dispersion qualitatively. However, the measured spectra are broader and slightly frequency – shifted due to finite angular aperture, unpolarized spectra detection, background emission, and fabrication imperfections. Therefore, more rigorous theoretical modeling is needed for further quantitative result analysis or further calibration of fabrication procedures.

6. References

[1] M. Lee *et al.*, “Photonic structures in radiative cooling,” *Light Sci. Appl.*, vol. 12, no. 1, p. 134, Jun. 2023, doi: 10.1038/s41377-023-01119-0.

[2] D. N. Basov, M. M. Fogler, and F. J. García de Abajo, “Polaritons in van der Waals materials,” *Science (1979).*, vol. 354, no. 6309, Oct. 2016, doi: 10.1126/science.aag1992.

[3] V. Janonis, A. Cernescu, P. Prystawko, R. Januškevičius, S. Indrišiūnas, and I. Kašalynas, “Near-Field Imaging of Hybrid Surface Plasmon-Phonon Polaritons on n-GaN Semiconductor,” *Materials*, vol. 18, p. 2849, Jun. 2025, doi: 10.3390/ma18122849.

[4] K. Jeganathan *et al.*, “Raman scattering of phonon-plasmon coupled modes in self-assembled GaN nanowires,” *J. Appl. Phys.*, vol. 105, no. 12, Jun. 2009, doi: 10.1063/1.3148862.

[5] V. Janonis, R. M. Balagula, I. Grigelionis, P. Prystawko, and I. Kašalynas, “Spatial coherence of hybrid surface plasmon-phonon-polaritons in shallow n-GaN surface-relief gratings,” *Opt. Express*, vol. 29, no. 9, p. 13839, Apr. 2021, doi: 10.1364/OE.423397.

[6] V. Janonis, S. Tumėnas, P. Prystawko, J. Kacperski, and I. Kašalynas, “Investigation of *n* -type gallium nitride grating for applications in coherent thermal sources,” *Appl. Phys. Lett.*, vol. 116, no. 11, Mar. 2020, doi: 10.1063/1.5143220.

[7] V. Janonis, J. Kacperski, A. Selskis, R. M. Balagula, P. Prystawko, and I. Kašalynas, “Directive and coherent thermal emission of hybrid surface plasmon-phonon polaritons in n-GaN gratings of linear and radial shapes,” *Opt. Mater. Express*, vol. 13, no. 9, p. 2662, Sep. 2023, doi: 10.1364/OME.494777.

[8] Charles. Kittel, *Introduction to solid state physics*, 8th ed. Wiley, 2005.

[9] J. D. Caldwell *et al.*, “Low-loss, infrared and terahertz nanophotonics using surface phonon polaritons,” *Nanophotonics*, vol. 4, no. 1, pp. 44–68, Dec. 2014, doi: 10.1515/nanoph-2014-0003.

[10] M. H. Wong *et al.*, “N-polar GaN epitaxy and high electron mobility transistors,” *Semicond. Sci. Technol.*, vol. 28, no. 7, p. 074009, Jul. 2013, doi: 10.1088/0268-1242/28/7/074009.

[11] L. Z. Tan, F. Zheng, S. M. Young, F. Wang, S. Liu, and A. M. Rappe, “Shift current bulk photovoltaic effect in polar materials-hybrid and oxide perovskites and beyond,” Aug. 2016, *Nature Publishing Group*. doi: 10.1038/npjcompumats.2016.26.

[12] C. R. Gubbin, S. De Liberato, and T. G. Folland, “Surface phonon polaritons for infrared optoelectronics,” *J. Appl. Phys.*, vol. 131, no. 3, Jan. 2022, doi: 10.1063/5.0064234.

[13] K. Feng *et al.*, “Localized surface phonon polariton resonances in polar gallium nitride,” *Appl. Phys. Lett.*, vol. 107, no. 8, Aug. 2015, doi: 10.1063/1.4929502.

[14] M. S. Dresselhaus, “SOLID STATE PHYSICS PART II Optical Properties of Solids.”

[15] J. D. Caldwell *et al.*, “Low-loss, infrared and terahertz nanophotonics using surface phonon polaritons,” *Nanophotonics*, vol. 4, no. 1, pp. 44–68, Apr. 2015, doi: 10.1515/nanoph-2014-0003.

[16] I. F. Almog, M. S. Bradley, and V. Bulovic, “The Lorentz oscillator and its applications,” *Massachusetts Institute of Technology*, pp. 8–41, 2011.

[17] W. L. Barnes, A. Dereux, and T. W. Ebbesen, “Surface plasmon subwavelength optics,” *Nature*, vol. 424, no. 6950, pp. 824–830, Aug. 2003, doi: 10.1038/nature01937.

[18] M. Kauranen and A. V. Zayats, “Nonlinear plasmonics,” *Nat. Photonics*, vol. 6, no. 11, pp. 737–748, Nov. 2012, doi: 10.1038/nphoton.2012.244.

[19] H. Raether, *Surface Plasmons on Smooth and Rough Surfaces and on Gratings*, vol. 111. Berlin, Heidelberg: Springer Berlin Heidelberg, 1988. doi: 10.1007/BFb0048317.

[20] P. McArdle, D. J. Lahneman, A. Biswas, F. Keilmann, and M. M. Qazilbash, “Near-field infrared nanospectroscopy of surface phonon-polariton resonances,” *Phys. Rev. Res.*, vol. 2, no. 2, p. 023272, Jun. 2020, doi: 10.1103/PhysRevResearch.2.023272.

[21] Z. Shi *et al.*, “Guided-Mode Resonances in GaN Membrane Grating,” *IEEE Photonics J.*, vol. 6, no. 3, pp. 1–7, Jun. 2014, doi: 10.1109/JPHOT.2014.2326680.

[22] Y. M. Lyaschuk, S. M. Kukhtaruk, V. Janonis, and V. V. Korotyeyev, “Modified rigorous coupled-wave analysis for grating-based plasmonic structures with a delta-thin conductive channel: far- and near-field study,” *Journal of the Optical Society of America A*, vol. 38, no. 2, p. 157, Feb. 2021, doi: 10.1364/JOSAA.410857.

[23] Z. Lokar, B. Lipovsek, M. Topic, and J. Krc, “Performance analysis of rigorous coupled-wave analysis and its integration in a coupled modeling approach for optical simulation of complete heterojunction silicon solar cells,” Aug. 2018. doi: 10.3762/bjnano.9.216.

[24] K. KODATE, “Rigorous Coupled-Wave Theory and its Application for Design of Diffractive Optical Elements,” *The Review of Laser Engineering*, vol. 36, no. 10, pp. 635–642, 2008, doi: 10.2184/lsj.36.635.

[25] S. A. Maier, *Plasmonics: Fundamentals and Applications*. New York, NY: Springer US, 2007. doi: 10.1007/0-387-37825-1.

[26] S. C. H. Allen Taflove, “Computational Electrodynamics The Finite-Difference Time-Domain Method,” *Computational Electrodynamics The Finite-Difference Time-Domain Method*, vol. 3rd, 2005.

[27] JIAN-MING JIN, *The Finite Element Method in Electromagnetics*, 2nd ed. John Wiley & Sons, 2002.

[28] D. I. S. Charalambos C. Katsidis, “General transfer-matrix method for optical multilayer systems with coherent, partially coherent, and incoherent interference,” *Appl. Opt.*, vol. 41, 2002.

[29] F. J. García de Abajo and A. Howie, “Retarded field calculation of electron energy loss in inhomogeneous dielectrics,” *Phys. Rev. B*, vol. 65, no. 11, p. 115418, Mar. 2002, doi: 10.1103/PhysRevB.65.115418.

[30] B. H. L. Novotny, *Principles of Nano-Optics*, 2nd ed. Cambridge University Press, 2012.

[31] K. Song, J. Wang, and G. Wang, “Rigorous Coupled-Wave Analysis Algorithm for Stratified Two-Dimensional Gratings with Unconditionally Stable H-Matrix Methods,” *Photonics*, vol. 12, no. 9, p. 943, Sep. 2025, doi: 10.3390/photonics12090943.

[32] S. Foteinopoulou, G. C. R. Devarapu, G. S. Subramania, S. Krishna, and D. Wasserman, “Phonon-polaritonics: enabling powerful capabilities for infrared photonics,” *Nanophotonics*, vol. 8, no. 12, pp. 2129–2175, Jun. 2018, doi: 10.1515/nanoph-2019-0232.

[33] Y. Xiao *et al.*, “Measuring Thermal Emission Near Room Temperature Using Fourier-Transform Infrared Spectroscopy,” *Phys. Rev. Appl.*, vol. 11, no. 1, p. 014026, Jan. 2019, doi: 10.1103/PhysRevApplied.11.014026.

[34] Bruker Optik GmbH, “VERTEX 70 User Manual .”

santrauka

Šiame darbe tiriami hibridiniai paviršiniai plazmonų–fononų polaritonai (SPPhP), sužadinami skirtingai legiruotose galio nitrido (GaN) paviršinėse gardelėse. Infraraudonųjų spindulių fotonika yra svarbi spektroskopijai, terminiam vaizdinimui, cheminiam jutikliavimui, selektyviajai šiluminei emisijai, radiaciniam aušinimui ir vidurinės infraraudonosios srities fotoniniams įrenginiams. GaN yra tinkama medžiaga, nes tai polinis puslaidininkis, turintis infraraudonojoje srityje aktyvius optinius fononus. Šie fononai leidžia susidaryti paviršiniams fononų polaritonams Reststrahlen juostos srityje. Legiruotame GaN laisvieji krūvininkai suteikia papildomą plazmoninį indėlį į dielektrinę funkciją, todėl fononai ir plazmonai gali sąveikauti ir sudaryti hibridines SPPhP modas.

Darbo tikslas – ištirti, kaip legiravimo lygis, užpildymo faktorius, gardelės geometrija ir kampinės surinkimo sąlygos veikia SPPhP rezonansų spektrinę elgseną. Buvo tiriami du n tipo GaN mėginiai su skirtingomis laisvųjų krūvininkų koncentracijomis. Abiejuose mėginiuose buvo suformuotos linijinės ir apskritiminės paviršinės gardelės, kurių periodas buvo 17,5 μm, o aukštis apie 1 μm. Buvo nagrinėti 25%, 50% ir 75% užpildymo faktoriai.

Šiluminės emisijos matavimai atlikti naudojant Bruker Vertex 70 FTIR spektrometrą. Įkaitinti GaN mėginiai veikė kaip infraraudonosios spinduliuotės šaltiniai. Kadangi optinė sistema turėjo baigtinę kampinę apertūrą ir nebuvo naudojamas išorinis poliarizatorius, išmatuoti spektrai buvo kampiškai vidurkinti ir iš esmės nepoliarizuoti. Tai svarbu, nes SPPhP rezonansai daugiausia susiję su TM poliarizacija ir priklauso nuo kampo.

Eksperimentiniai spektrai buvo apdoroti taikant bazinės linijos korekciją ir normalizaciją, o vėliau palyginti su RCWA teoriniais skaičiavimais. Rezultatai parodė, kad abu mėginiai palaiko SPPhP šiluminės emisijos ypatybes netoli apatinės GaN Reststrahlen juostos ribos. Didesnio legiravimo mėginys parodė stipresnius ir aiškesnius rezonansus, o mažesnio legiravimo mėginyje rezonansai buvo platesni ir mažiau aiškūs. Skirtumai tarp eksperimento ir teorijos siejami su kampine apertūra, nepoliarizuotu matavimu, fonine emisija, gamybos netobulumais ir idealizuotu RCWA modeliu.